

3. SITE 1044¹

Shipboard Scientific Party²

HOLE 1044A

Position: 15°32.3924'N, 58°38.4766'W

Date occupied: 2100 hr, 26 December 1996

Spud hole: 1400 hr, 27 December 1996

End hole: 0200 hr, 30 December 1996

Time on hole: 3 days, 5 hr

Seafloor Depth (drill-pipe measurement from rig floor, m): 4983

Distance between rig floor and sea level (m): 11.0

Water depth (drill-pipe measurement from sea level, m): 4972

Total depth (from rig floor, m): 5668

Penetration (m): 685

Total core recovered (m): 0

Comments: Logging while drilling (LWD). No coring done. Seafloor depth identified from LWD data.

Principal results: Drilling at Site 1044 penetrated through 685 m of sediment to basaltic basement of the North American Plate at 6 km east of the frontal thrust of the northern Barbados accretionary prism. LWD acquired gamma-ray, resistivity, density, caliper, photoelectric effect, and neutron porosity logs in the hole (Fig. 1; also see Fig. 2 [back-pocket foldout, this volume]). Excluding neutron porosity, all logs are of good quality because of an in-gauge hole. Ninety-nine percent of the hole had differential caliper measurements of <1 in, and 94% measured <0.5 in. The density log mimics both the character and values of density measurements made from cores, further indicating log reliability (Fig. 12).

Both traditional visual and multivariate statistical analyses of the logs define six log units that account for the majority of the lithologic variation observed in the cores (Fig. 9). This profile of log properties specifies the nature of the incoming sedimentary section and correlates well with the 3-D seismic survey and with Site 672, which is located ~35 m from Site 1044. This core-log-seismic data suite provides an unparalleled reference for analysis of the evolution of the accretionary prism to the west.

A decrease in density, resistivity, and gamma ray on the logs from 169 to 189 m below seafloor (mbsf) defines log Unit 2, which correlates well with a structurally defined proto-décollement zone (Fig. 1). This low-density unit is recognizable in both the logs and cores, but because of incomplete core recovery, logs better define its discrete boundaries and correlate it with a radiolarian mudstone interval at Site 672. A stratigraphically correlative mudstone interval always characterizes the décollement zone beneath the accretionary prism (Masle and Moore, 1990; Masle, Moore, et al., 1988). Consolidation tests on cores from Site 672 suggest high fluid pressures in this low-density zone that would favor deformation (Taylor and Leonard, 1990). The logs show no evidence in the proto-décollement zone for extreme fluid pressures that might produce hydrofractures, and the geochemical evidence for fluid flow is equivocal here

(Fig. 17). The synthetic seismogram based on log results shows that this low-density interval would have a reflection similar to that seen beneath much of the accretionary prism (Fig. 18). Thus, the incipient structures, physical properties, stratigraphic correlation, and seismic character all confirm that log Unit 2 is the proto-décollement zone.

Significant spikes in caliper, bulk density, resistivity, and photoelectric effect, a decrease in gamma-ray, and an increase in resistivity values define log Unit 4 from 330 to 470 mbsf. This unit correlates with cyclically bedded sediments with high concentrations of sand and carbonate at Site 672. Anomalies in pore-fluid geochemistry suggest fluid flow in this unit. Lithologic properties derived from the logs indicate sand layers that could act as fluid conduits. A synthetic seismogram generated from the logs correlated through the 3-D seismic survey shows that this unit extends beneath the accretionary prism, enabling long-distance lateral migration of fluids.

BACKGROUND AND OBJECTIVES

Site 1044 is on the northern flank of the Tiburon Rise, about 6 km east of the frontal thrust, ~35 m bearing 259° from Site 672 (Fig. 2 [back-pocket foldout, this volume]; also see Fig. 3 for location of seismic line 751). Site 672 was drilled as an undeformed reference locality to gauge changes in the sedimentary section caused by accretion or underthrusting observed at other Deep Sea Drilling Project (DSDP) and Ocean Drilling Program (ODP) sites to the west. Surprisingly, the structural and geochemical anomalies at the projected stratigraphic level of the décollement zone suggested that the section at Site 672 is disturbed by the encroaching accretionary prism (Shipboard Scientific Party, 1988). Drilling at Site 672 provided valuable baseline information on the nature of the incoming sedimentary section and set new limits on the possible extent of proto-décollement zone deformation.

Site 672 provides a wealth of information for correlation with the LWD data acquired at Site 1044. Cores at DSDP Site 543, located 18 km north on the oceanic plate (see Fig. 1 in "Faulting, Fluid Flow, and Seismic Imaging of the Northern Barbados Subduction Zone" chapter, this volume), constrain the nature of the lower Eocene to Cretaceous part of the section that was not penetrated at Site 672 (Shipboard Scientific Party, 1984). The sedimentary section is about 650 m thick beneath Site 672 and overlies oceanic crust of probable Cretaceous age. The uppermost Pleistocene to lower Miocene hemipelagic unit extends to about 200 mbsf and is equivalent to the section that is incorporated in the accretionary prism. This upper 200-m section correlates to seismic Unit 1 of moderately continuous reflectors and is underlain by a strong, positive polarity reflector (Fig. 4). At Site 672, the proto-décollement zone occurs at ~170–200m sub-bottom but shows no deformation at the resolution of the seismic data. Below the proto-décollement zone, upper Oligocene to middle Eocene units consist of alternating muddy and calcareous lithologies with sandstone and siltstone interbeds indicative of terrigenous input. The lower middle Eocene to Cretaceous rocks are siliceous, calcareous, and clay-rich pelagic deposits overlying pillow basalt.

The principal questions addressed at Site 1044 are

¹Moore, J.C., Klaus, A., et al., 1998. *Proc. ODP, Init. Repts.*, 171A: College Station, TX (Ocean Drilling Program).

²Shipboard Scientific Party is given in the list preceding the Table of Contents.

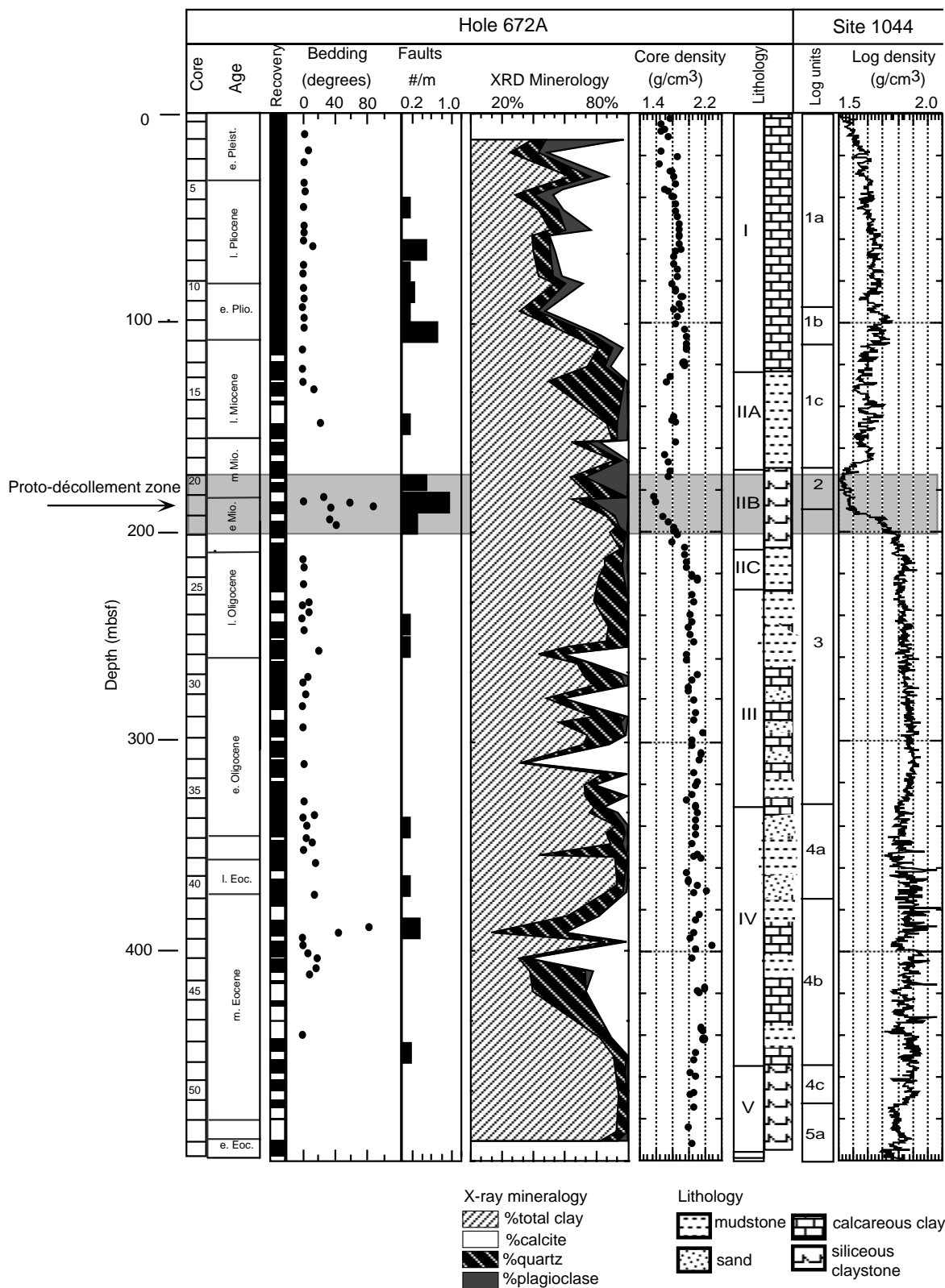


Figure 1. Data synthesis showing the relationship between Leg 110 Hole 672A (Shipboard Scientific Party, 1988) core data and Leg 171A Site 1044 LWD data.

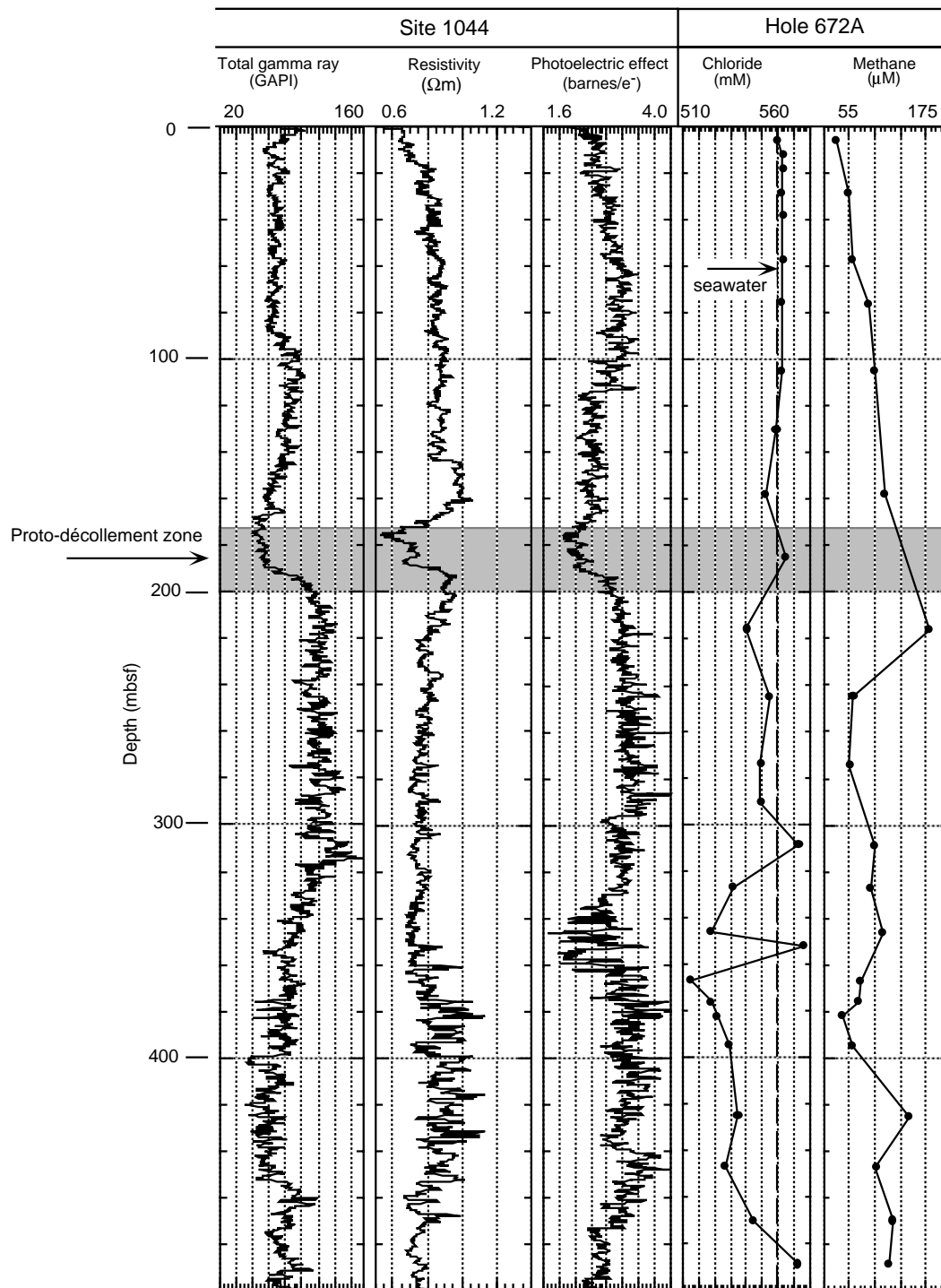


Figure 1 (continued).

1. What is the log signature of the proto-décollement zone? Does this deformation zone include any indicators of hydrofractures?
2. What are the overall physical properties, especially porosity, of the incoming section? This question is important because equivalents of this sequence are the sources of fluids being expelled from the accretionary prism and underthrust sequence.
3. How do the observed physical properties determined from LWD account for the seismic reflection signature of this well-imaged incoming sedimentary section?

OPERATIONS

Transit to Site 1044

The last line was cast off from Pier 18 at Balboa, Panama, at 0300 hr, 20 December 1996, and the vessel commenced sea voyage east through the Panama Canal. Because of heavy traffic, the vessel waited at anchor for 13 hr in Gatun Lake until clearance was received to pass through the Gatun Locks. After exiting the canal and entering the Caribbean, moderate seas (8–12 ft) and winds (25–30 kt) held the

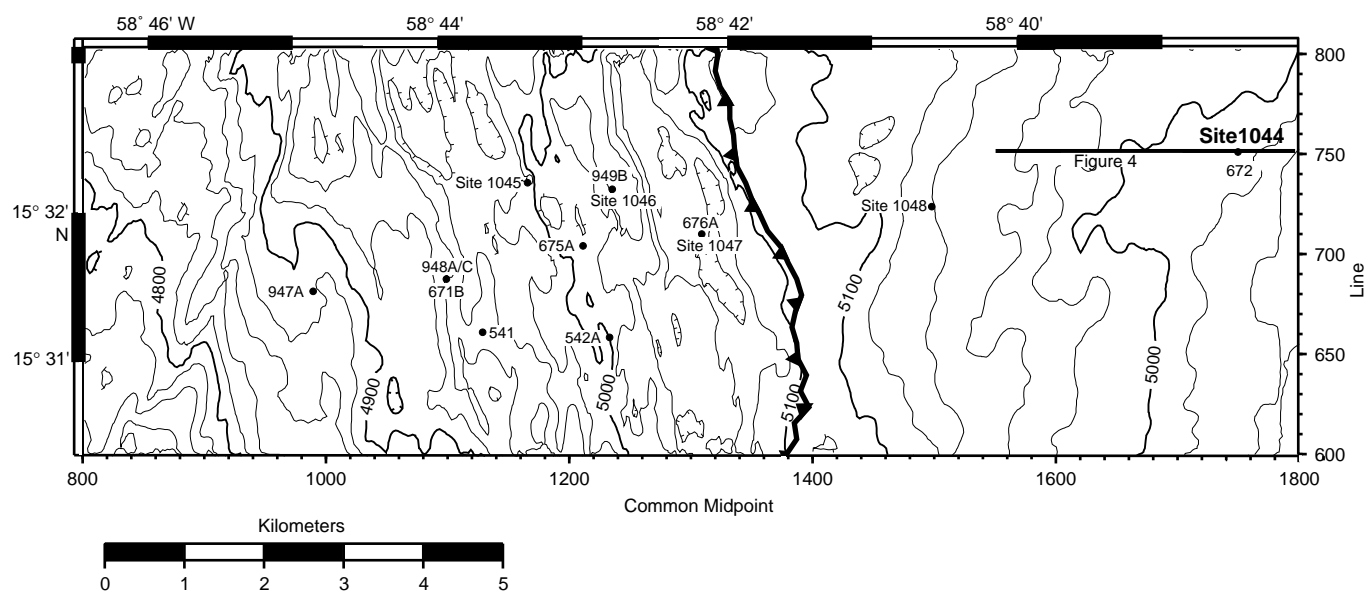


Figure 3. Bathymetric location map for Site 1044 in the Leg 171A drilling area and for previous ODP and DSDP holes in the northern Barbados accretionary prism.

vessel speed under 8 kt for 2 days. Improved weather and sea states allowed better progress toward the end of the transit to Site 1044. The vessel arrived at the first site, Site 1044, at 2100 hr on 26 December, after a transit of 1371 nmi at an average speed of 9.1 kt.

Hole 1044A

LWD Hole 1044A was located at Global Positioning System (GPS) coordinates 15°32.3965'N, 58°38.4793'W. This location is at a range of 35 m and a bearing of 259° from Site 672. The location of Hole 1044A was based on the 3-D seismic reflection survey and the final site position for Site 672, which was produced by averaging transit satellite fixes. The *JOIDES Resolution* GPS navigation data were automatically corrected to the moonpool using the ship's heading (gyro compass) and the known offset of the GPS antenna from the moonpool. Upon arrival at the desired drill site GPS coordinates, a beacon was deployed. After the beacon had settled to the seafloor and while we were tripping pipe to the seafloor, the ship was stabilized over the beacon using the ship's dynamic positioning system. The GPS data collected during the pipe trip to the seafloor were averaged, and we offset from the beacon location before spudding the hole to ensure that the ship was in the desired location with respect to the 3-D seismic data. After the hole was spudded into the seafloor, GPS data collected during drilling were averaged over an ~48-hr period to calculate the final site position.

The LWD bottom-hole assembly (BHA) consisted of a used 9⁷/₈-in Smith FDGH (3 × 14) bit, LWD bit sub, LWD compensated density resistivity (CDR) tool, double-pin LWD crossover, LWD compensated density neutron (CDN) tool, LWD crossover sub, eight 8¹/₄-in drill collars, crossover, Bowen down jars, Bowen up jars, crossover, two 8¹/₄-in drill collars, a tapered drill collar (TDC), and six joints of 5¹/₂-in drill pipe.

Hole 1044A was spudded at 1400 hr, 27 December 1996. Drilling was initiated at 25 m/hr at a water depth of 4991.4 m below rig floor (mbrf), based on the precision depth recorder (PDR) reading. It was not possible to determine the mudline with the drill pipe in the soft hemipelagic sediments. Therefore, the PDR reading of 4991.4 mbrf was used for the water depth, and the actual water depth was obtained after analyzing the LWD data. Drilling continued at 25 m/hr to 5291 mbrf (300 mbsf), where a precautionary wiper trip was made. The

proto-décollement zone was estimated to be at a depth of ~200 mbsf, and the wiper trip was made from 300 to 160 mbsf to allow the top of the BHA to clear the seafloor and also to ream the hole in the location of the décollement zone. No drag or hole problems occurred during the wiper trip. A 30-barrel sweep of sepiolite mud was used to clean out 9 m of fill that had accumulated at the bottom of the hole, and drilling resumed at 25 m/hr. The rate of penetration (ROP) was increased to 35 m/hr at 5379 mbrf (388 mbsf) to finish the hole quickly. The drilling rate slowed significantly to 4 m/hr at a depth of 5663 mbrf, indicating that we had reached the basement. Hole 1044A was terminated at 5666 mbrf (675 mbsf), with the depth objective successfully achieved.

The drill string was raised to 5126 mbrf (135 mbsf) and the hole was displaced with 45 barrels of heavy (10.5 lb/gal) mud. The LWD tools were raised to the drill floor, where the nuclear sources were removed, and the LWD collars were laid out. The beacon was recovered, and the bit cleared the rotary table at 0200 hr on 30 December 1996 to end Hole 1044A.

CHARACTERIZATION OF LOGS

Definition of Log Units

An overview of the log data, with the log units labeled, is shown in Figure 5. Six first-order log units and several second-order units were defined through a combination of visual interpretation and multivariate statistical analysis (see "Explanatory Notes" chapter, this volume).

For multivariate statistical analysis, factor logs were calculated from the R_{ad} , gamma-ray, thorium, potassium, photoelectric effect, bulk density, and neutron porosity logs. The first three factor logs account for 88% of the total variance in the selected data. Cluster analysis of these three factor logs identifies five prominent clusters, each with a distinct set of log properties. Mean and standard deviation values of the log properties for each cluster are summarized in Table 1, and the distribution of clusters with depth is shown in Figure 6, together with the log units and LWD density and gamma-ray curves.

Log Unit 1 (0–169.2 mbsf) has a mean bulk density of 1.6 g/cm³ and low (0.04 g/cm³) standard deviation (Figs. 5, 6) and is subdivided into three subunits. The base of Subunit 1a (0–93.7 mbsf) has a pos-

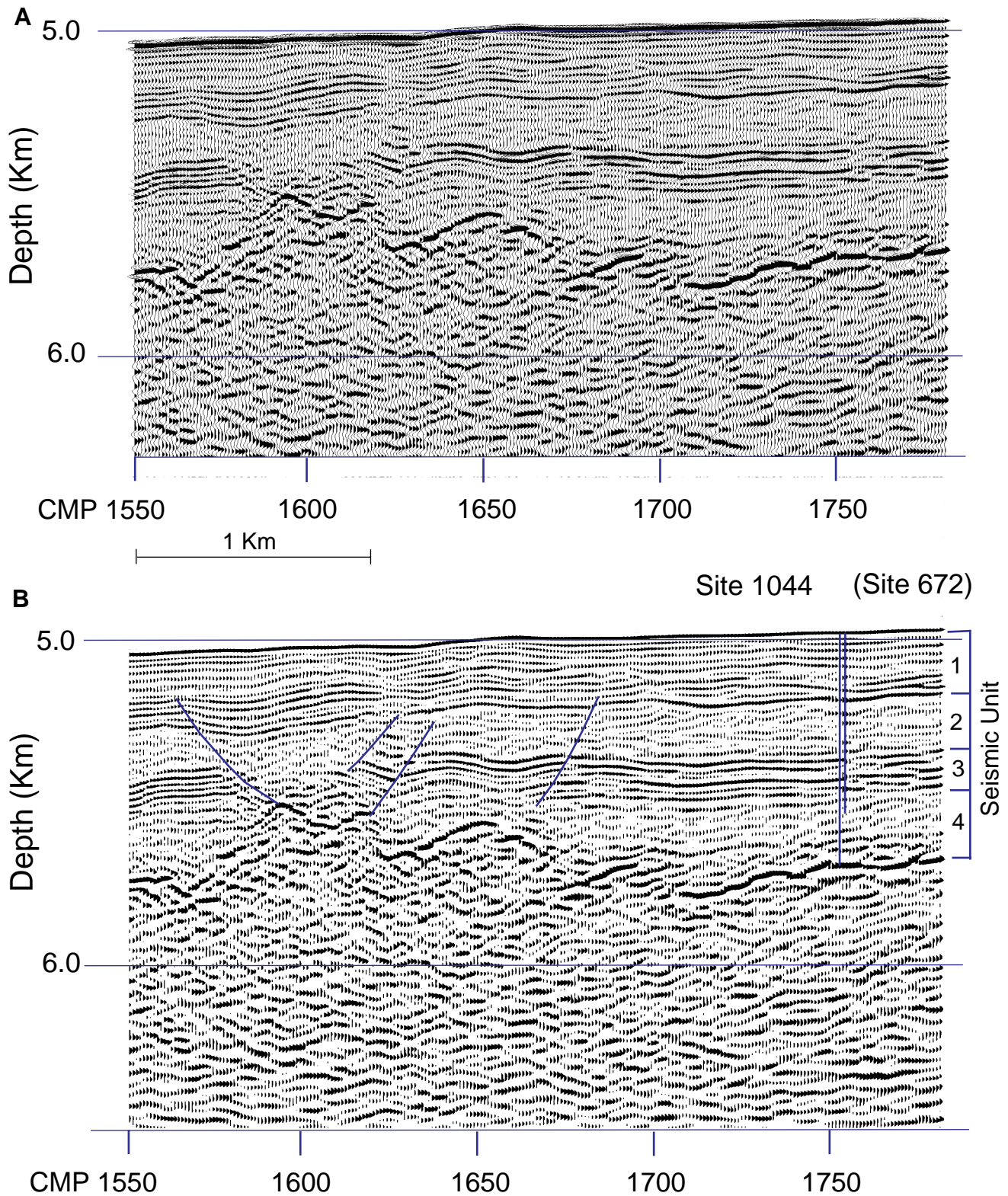


Figure 4. (A) Uninterpreted and (B) interpreted seismic Line 751 through Site 1044 (see Fig. 3 for location). Black is positive polarity; white is negative polarity. The seismic stratigraphic units shown to the right of the interpreted panel are after Moore et al. (1995).

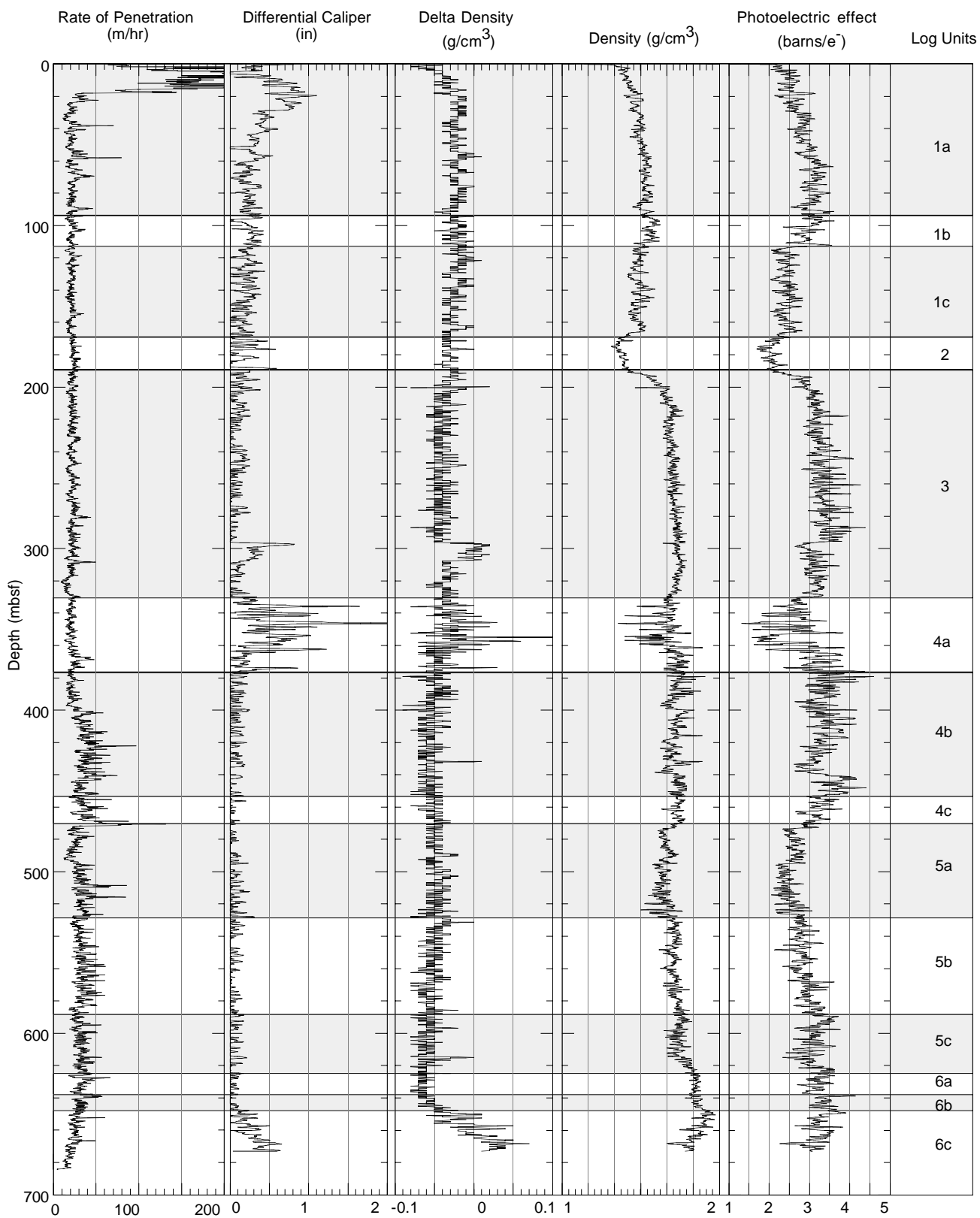


Figure 5. Site 1044 LWD data and interpreted log units. Post-cruise processed log data are available on CD-ROM (back pocket, this volume).

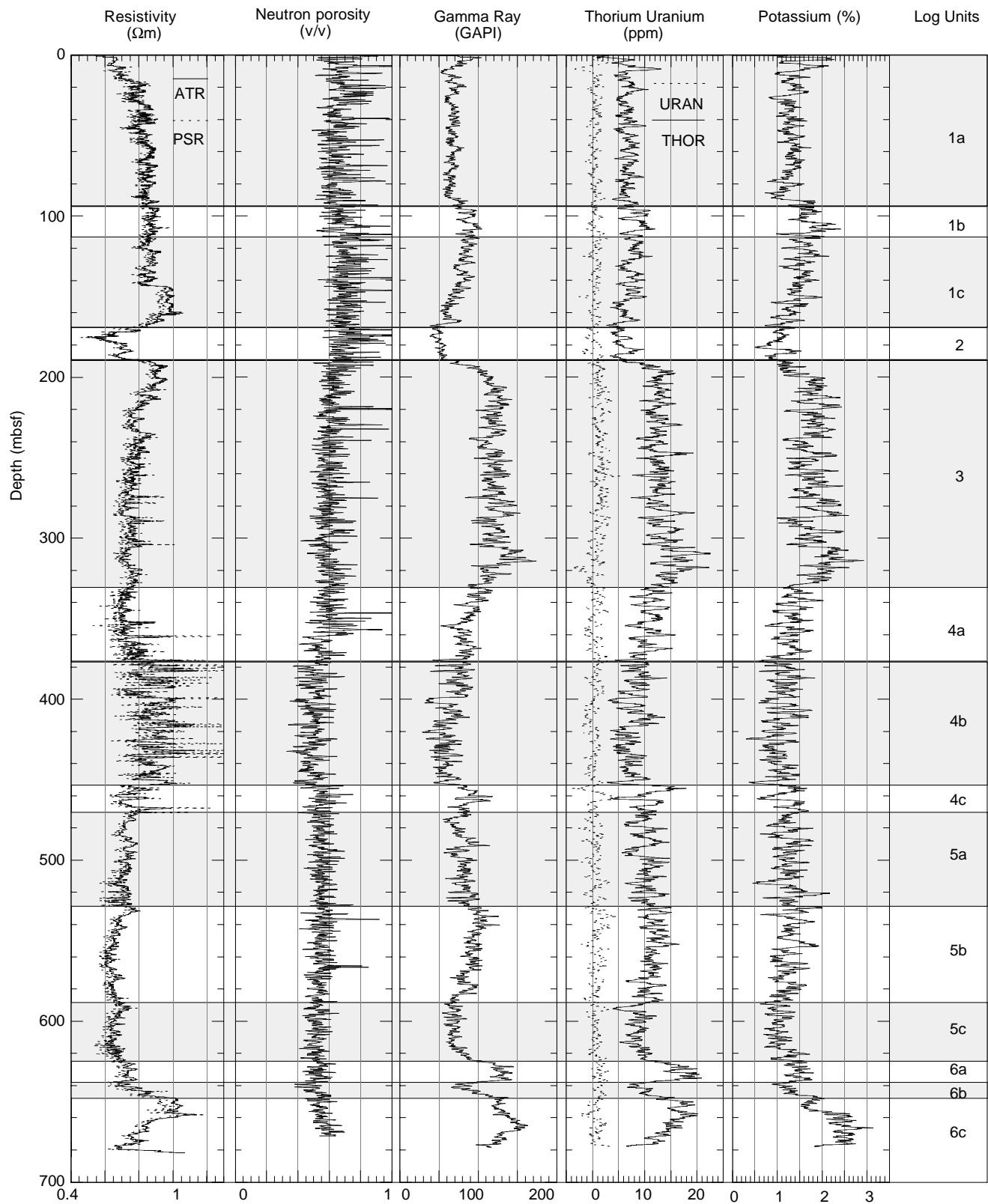


Figure 5 (continued).

Table 1. Mean values and standard deviations of the log properties according to each cluster for Hole 1044A.

	ATR (Ωm)		GR (GAPI)		THOR (ppm)		POTA (%)		PEF (barns/e ⁻)		ROMT (g/cm ³)		TNPH (v/v)	
	Mean	SD	Mean	SD	Mean	SD	Mean	SD	Mean	SD	Mean	SD	Mean	SD
Cluster 1	0.69	0.05	63.30	14.10	6.84	2.60	1.21	0.34	2.18	0.25	1.51	0.09	0.67	0.05
Cluster 2	0.87	0.06	70.90	9.50	6.88	1.40	1.35	0.21	2.71	0.33	1.60	0.04	0.69	0.04
Cluster 3	0.81	0.07	113.90	17.50	13.10	2.60	1.75	0.30	3.23	0.25	1.86	0.10	0.59	0.04
Cluster 4	0.70	0.04	84.20	12.20	10.40	1.90	1.23	0.24	2.83	0.31	1.84	0.06	0.55	0.03
Cluster 5	0.90	0.07	61.80	12.30	7.24	1.90	1.01	0.23	3.43	0.30	1.88	0.05	0.50	0.02

Notes: SD = standard deviation; ATR = deep resistivity; GR = gamma ray; THOR = thorium; POTA = potassium; PEF = photoelectric effect; ROMT = density (rotationally processed); TNPH = thermal neutron porosity.

itive shift in the gamma-ray and potassium logs. The base of Subunit 1b (93.7–113.7 mbsf) is at a major negative shift in the photoelectric effect log. Within Subunit 1c (113.7–169.2 mbsf) is a separation of about 0.05 Ωm between the shallow and the deep resistivity curves (Fig. 5) just above the proto-décollement zone (Fig. 5). Separation of the deep and shallow resistivities can occur because of invasion of conductive drilling mud into the formation. However, only seawater was used for drilling (no drilling mud was used), and invasion is assumed to be negligible. See the “Logs and Lithology” section (this chapter) for further discussion of the resistivity anomaly.

Log Unit 2 (169.2–189.3 mbsf), the proto-décollement zone, is characterized by significant negative shifts of mean values (Figs. 5, 6; Table 1) of 0.09 g/cm³ in bulk density, 0.18 Ωm in deep resistivity, 7.6 GAPI in gamma ray, and 0.53 barns/e⁻ in photoelectric effect.

Log Unit 3 (189.3–330.0 mbsf) is characterized by large positive shifts of mean values (Figs. 5, 6; Table 1) of 0.35 g/cm³ in bulk density, 0.12 Ωm in deep resistivity, 50.6 GAPI in gamma ray, and 1.05 barns/e⁻ in photoelectric effect.

Log Unit 4 (330.0–470.5 mbsf) shows high variability in the caliper, bulk density, resistivity, neutron porosity, and photoelectric effect logs. Subunit 4a (330.0–376.6 mbsf) has a high differential caliper variability (range of 0 to 2 in), creating spikes in the unedited bulk density log. It also has a gradual decrease in neutron porosity and gamma ray, and the photoelectric effect is highly variable (standard deviation of 0.3 barns/e⁻). Subunit 6 (376.6–453.1 mbsf) contains a substantial number of positive resistivity spikes greater than 1.2 Ωm . The top of Subunit 4c (453.1–470.5 mbsf) is defined by an increase in neutron porosity and gamma ray. The Unit 4/5 boundary is defined by decreases in photoelectric effect and bulk density.

Log Unit 5 (470.5–624.5 mbsf) is characterized by a gradual increase in bulk density from 1.8 to 2.0 g/cm³ throughout the interval and by less variation in the resistivity and photoelectric effect logs, compared with Unit 4. The bottom of Subunit 5a (470.5–528.2 mbsf) is defined by an increase in resistivity variability and an increase in variability in bulk density. The bottom of Subunit 6 (528.2–588.6 mbsf) represents an increase in resistivity to 0.7 Ωm . Subunit 5c (588.6–624.5 mbsf) is characterized by gradual increases in the gamma-ray and bulk density logs. The Unit 5/6 boundary is marked by a significant positive gamma-ray shift of 29.4 GAPI and a photoelectric effect shift of 0.4 barns/e⁻.

Log Unit 6 (624.5–671.5 mbsf) is defined primarily by the gamma-ray log. Subunit 6a (624.5–638.2 mbsf) is a short interval of high gamma ray (median of 113.9 GAPI), followed by Subunit 6b (638.2–647.2 mbsf), a short interval of low gamma ray (median of 84.2 GAPI). The Subunit 6b/6c boundary is defined as a positive shift in the gamma-ray mean value of 29.4 GAPI. Subunit 6c (647.2–671.5 mbsf) has high density and resistivity, and the differential caliper increases steadily from 0 to ~0.7 in.

Density Log Editing

The LWD density log was edited to eliminate the low-density spikes that are a result of poor hole conditions. Low-density spikes that coincide with high (>1 in) differential caliper values were replaced by averaging the surrounding density values.

LWD Log Quality

Figure 7 shows the quality control logs at Hole 1044A. Industry experience indicates that for the spectral gamma-ray measurements of the natural gamma-ray (NGT) tool, a 1.5-m averaged ROP of 20 m/hr produces good data, and 30 m/hr ROP produces marginal data. For ODP operations, a target ROP of 25 m/hr was chosen. However, this ROP could not be maintained in the uppermost section of Hole 1044A. An ROP >100 m/hr from 0 to 20 mbsf reduced resolution in the resistivity measurements in the first 17 m, NGT in the first 14 m, density in the first 9 m, and neutron porosity in the first 7 m. The ROP for the interval 20–400 mbsf was kept at 25 m/hr to maintain NGT data quality. Although the average ROP increased to 35 m/hr in the interval 400–685 mbsf, no significant baseline shift in the NGT was observed. The industry guideline is based on the environment of drilling fluid that is heavier than the seawater used as drilling fluid in ODP holes. Therefore, NGT data at ROPs higher than 30 m/hr are apparently reliable in the environment of light drilling fluid.

The differential caliper is the best indicator for borehole conditions. A standoff of <1 in between the tool and borehole wall indicates good borehole conditions and maintains a bulk density accuracy of ± 0.015 g/cm³. The differential caliper values in Hole 1044A show <1-in standoff—except for one interval at 20 mbsf and several small intervals at 335–362 mbsf. The largest value of 2 in occurs at 346 mbsf. Zones of minor washout are identified in intervals at 0–30, 297–307, 335–362, and 650–672 mbsf. The increased ROP reduced the standoff below 400 mbsf. Overall, the borehole condition is excellent. A differential caliper of <1 in was measured in 99.3% of the hole, and 93.8% is <0.5 in. The bulk density correction (DRHO), calculated from the difference between the short- and long-spaced density measurements, varies from -0.1 to 0.1 g/cm³, which shows the high quality of the density measurements. Time-after-bit (TAB) measurements are 10 to 40 min for resistivity and gamma-ray measurements and 30 to 80 min for density and neutron porosity measurements. High TAB values of as much as 200 min at the interval 297–307 mbsf coincide with a wiper trip. However, the differential caliper and DRHO logs indicate that the section of the borehole that had been drilled, but not measured, at the time of the wiper trip did not deteriorate significantly.

LOGS AND LITHOLOGY

Hole 1044A was drilled ~35 m from Site 672, which is sufficiently close to correlate the logged section with recovered sediments. Lithologies from Site 672 are summarized below, along with bulk mineralogy from shipboard and shore-based X-ray diffraction (XRD) analyses. A more detailed description of the sedimentary units, depositional environments, and core photographs are in the Leg 110 *Initial Reports* volume (Masle, Moore, et al., 1988). The lower Paleogene and Cretaceous parts of the logged section (below 500 mbsf) are compared with Site 543 (DSDP Leg 78A; Biju-Duval, Moore, et al., 1984), which is located 18 km to the north, also in a position well away from the thrust front. Figure 8 summarizes the correlation between Site 1044 and the previously drilled holes.

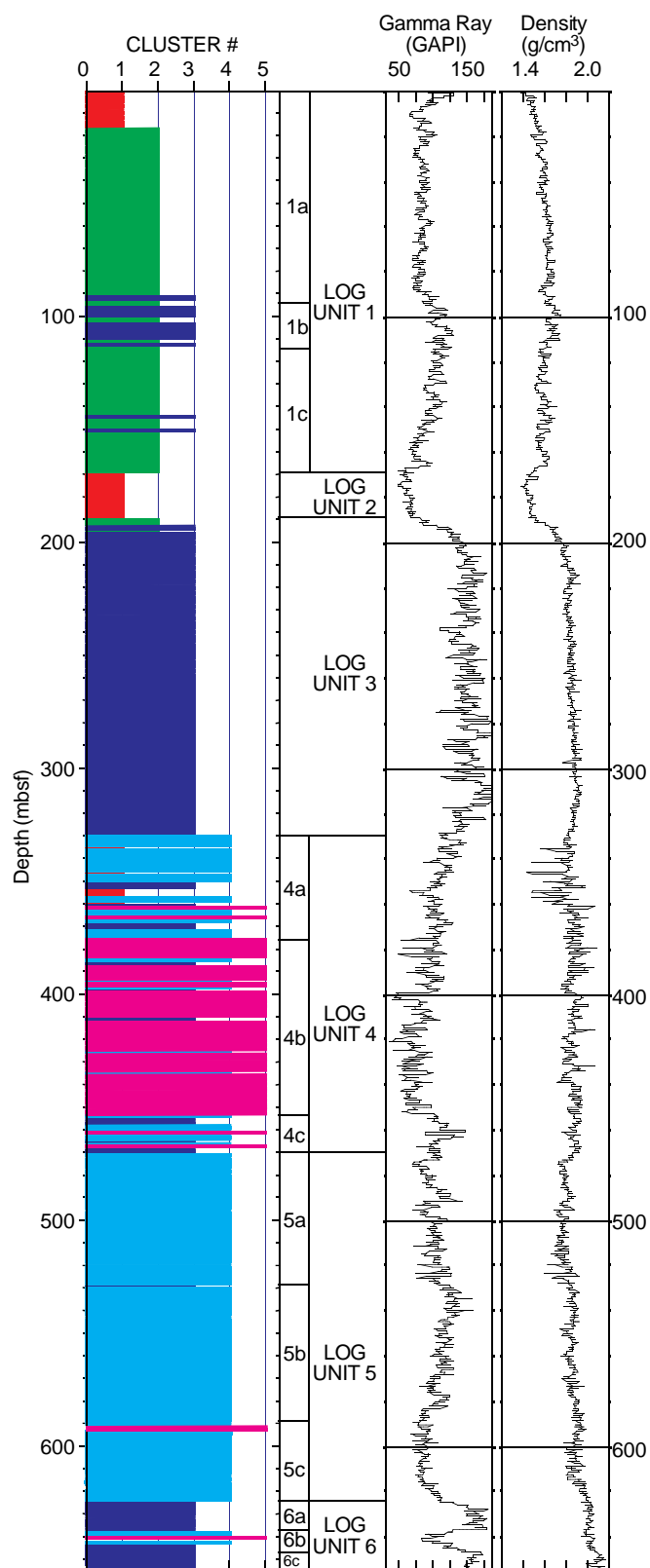


Figure 6. Definition of log units for Site 1044. Five clusters were derived from three factor logs accounting for 88% of the total variance observed in the data. Boundaries between the first-order log units correspond to changes in log character related primarily to lithology that are clearly visible on the logs (e.g., gamma ray, density, photoelectric effect, and resistivity). Second-order units represent subtle changes in log character that are observed in only a few curves and that may not be related to lithology.

Sediments from Site 672 were divided into five lithologic units. Units I, II, and V are characterized by relatively homogeneous hemipelagic sedimentation, whereas Units III and IV are composed of cyclic alternations of three or four different lithologies reflecting a significant influx of terrigenous material and possible redeposition by a variety of mechanisms. Sedimentation rates based on biostratigraphic age assignments indicate moderate accumulation rates for Units I and III, low accumulation rates for Units II and V, and high accumulation rates for Unit IV.

Site 672

Lithologic Unit I (0–123.3 mbsf)

Lithologic Unit I comprises lower Pleistocene to upper Miocene pale yellowish brown to greenish gray calcareous clay, calcareous mud, and marl. Ash layers are present throughout Unit I and are commonly highly bioturbated.

Lithologic Unit II (123.3–227.8 mbsf)

The transition to lithologic Unit II is marked by a sharp decline in the carbonate content of the sediments to nearly zero. Unit II is further divided into three subunits. Subunit IIA (123.3–170.8 mbsf) is composed of green and olive gray mud/siltstone and clay/claystone of late Miocene age. Ash beds are less common than in Unit I, and where present, they are commonly bioturbated, although the overall intensity of bioturbation is less than that observed in Unit I.

Subunit IIB (170.8–208.8 mbsf) is characterized by a higher ash content than the remainder of the unit, as well as a significant siliceous component (5%–15% radiolarians and sponge spicules). The age determinations and lithology of Subunit IIB suggest that it is equivalent to the décollement zone of Site 671. Subunit IIC (208.8–227.8 mbsf) comprises mildly bioturbated mudstones. These sediments are clay rich, containing 80% to 90% total clay minerals. They are calcite free and contain 10% to 20% quartz and 5% plagioclase.

Lithologic Unit III (227.8–332.3 mbsf)

Lithologic Unit III is characterized by marlstones interbedded with claystones, mudstones, and siltstones of variable carbonate content. Both sharp and gradational contacts are present between the different lithologies; however, gradational contacts between claystone, mudstone, and siltstone are common in the upper part of the section. The lower part of the section is characterized by nannofossil clay layers with sharp basal boundaries that grade upward into, or are overlain with, sharp contacts by a less calcareous lithology.

Lithologic Unit IV (332.3–455.8 mbsf)

The sediments of lithologic Unit IV are also cyclically bedded and are distinguished from Unit III by the presence of intercalated, pale green to gray quartz sandstones. Sediment ages range from middle Eocene to late Eocene or early Oligocene. The sandstone layers are calcareous and glauconitic and range in thickness from 1 to 60 cm. These beds commonly contain a mixture of very fine-grained silt and sand-sized quartz. The sandstones are interlayered with dark green noncalcareous claystone and olive, brown, and dark gray mudstones and siltstones with variable carbonate content. The calcareous quartz sandstones and marlstones commonly have sharp basal contacts and parallel laminae, and they grade upward into claystones.

Lithologic Unit V (455.8–493.8 mbsf)

Lithologic Unit V consists of slightly siliceous claystones/mudstones of early to middle Eocene age. Carbonate content is negligible. Unit V exhibits numerous color changes from dark green to brown to reddish brown. Radiolarian content varies from 5% to 30%, and traces of quartz silt are dispersed throughout the unit. Unit V sediments show no evidence of bioturbation.

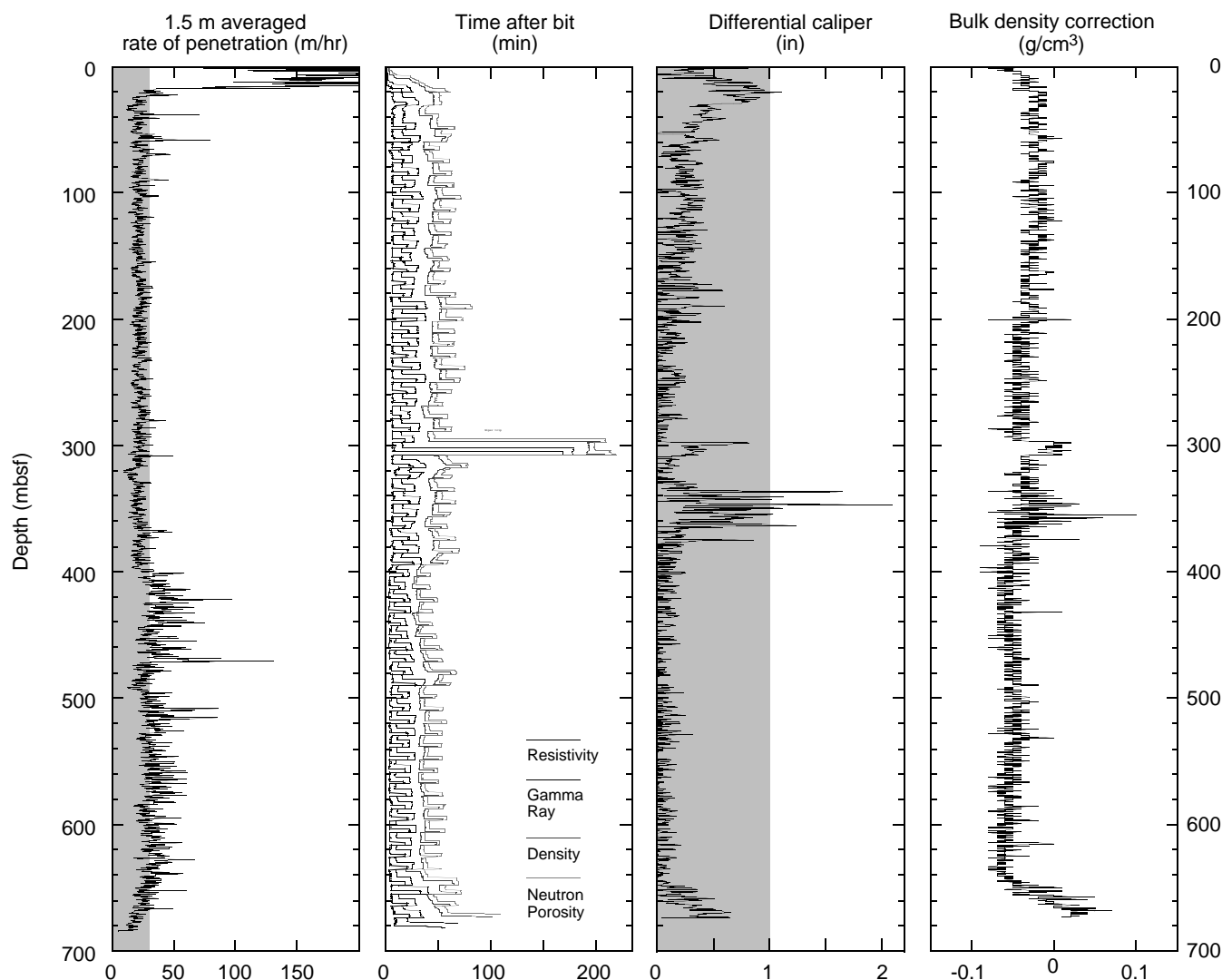


Figure 7. Summary of the quality-control logs. The shaded area in the ROP shows the reliable zone for NGT measurements according to industry experience. The shaded area in the differential caliper indicates good borehole conditions.

Bulk Mineralogy

The trends observed in the bulk mineralogy column of Figure 9 can generally be related to the changing influence of hemipelagic sedimentation vs. lateral influxes of terrigenous and calcareous sediment, with intermittent deposition of volcanic ash from the Lesser Antilles Arc.

The percentage of total clay minerals in the upper 100 m of the section varies widely between 20% and 60%, with an average of about 40%. From 100 to 190 mbsf, the percentage of total clay increases to between 80% and 90%. This high clay content is characteristic for the interval from 190 to 250 mbsf. It reflects hemipelagic sedimentation and corresponds to lithologic Units I and II and the uppermost part of Unit III. From 250 to 476 mbsf the clay content reflects the alternations in lithology of Units III and IV. The lower part of the middle Eocene section marks a return to dominantly hemipelagic sedimentation (456–494 mbsf). The siliceous clay/mudstones of this unit have a total clay content ranging from 82% to 94%.

Sharp fluctuations in the percentage of calcite occur throughout Unit I sediments, with average values increasing slightly with depth from ~0%–25% to about 40% at a depth of 80 mbsf. Below 80 mbsf, calcite content decreases until the section becomes calcite free at the

base of Unit I (123 mbsf). Calcite reappears at 252 mbsf in Unit III. The calcite content of the sediments in Units III and IV is highly variable and largely reflects influxes of carbonate sediment. The carbonate-rich layers of Units III and IV are interbedded with noncalcareous claystone and mudstone layers. The upper portion of Unit IV (335–370 mbsf) and the sediments of Unit V are calcite free.

The plagioclase content of the samples reflects the occurrence of ash layers and dispersed ash. The quartz content varies between 2% and 23% in sediments from Units I and II. Most samples contain about 10% quartz, a value similar to that of the hemipelagic sediments in the upper 500 m of Site 671. Sediments from Units III and IV show widely varying quartz contents, reflecting the influence of terrigenous silts and sands.

Correlation With Log Units

The upper part of log Unit 1 correlates with the calcareous mud defined as lithologic Unit I. The increase in gamma-ray log at the top of log Subunit 1b (93.7 mbsf), which is driven by increases in the amounts of thorium and potassium, correlates with the increase in total clay evident in the XRD record and with the core description from Site 672. A marked decrease in the photoelectric effect log at the bot-

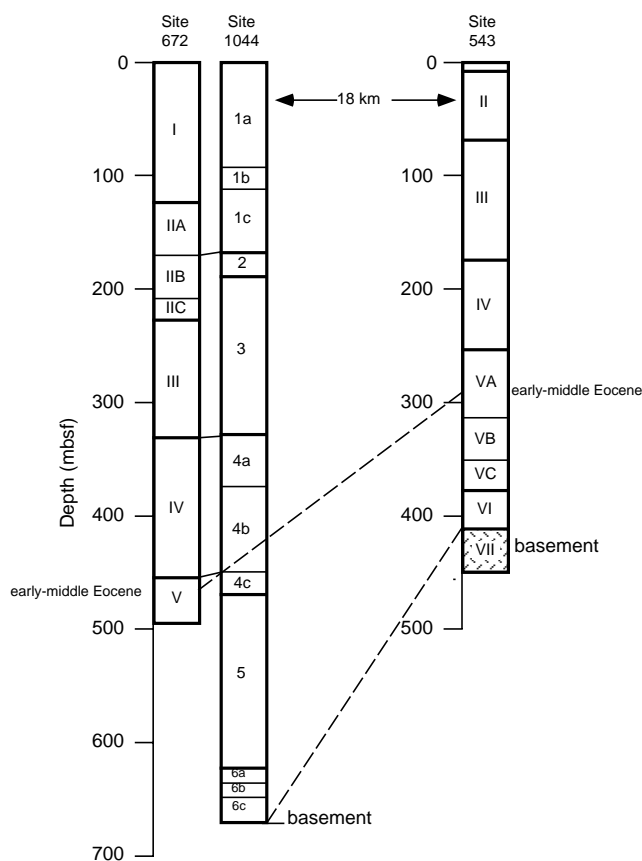


Figure 8. Correlation of log units defined at Site 1044 with lithologic units defined at Sites 672 and 543. Dashed lines indicating tie points between the sites represent time-equivalent horizons.

tom of log Subunit 1b (113.7 mbsf) correlates with an abrupt drop in carbonate content and with an increase in quartz. This corresponds approximately to the boundary between lithologic Units I and II. There is no evidence in the logs (e.g., thorium or resistivity peaks) of the high ash content present in the cores throughout the Unit I interval.

The bottom part of log Subunit 1c shows an abrupt increase in resistivity of about $0.1 \Omega\text{m}$ occurring at about 143 mbsf. In this interval the shallow and deep resistivities show a clear separation, with deep resistivity showing higher values. This phenomenon is not readily explained by bedding dip or formation anisotropy, which are common causes of offsets between deep and shallow resistivity and generally result in higher shallow resistivity. Fluid invasion also seems an unlikely explanation, given the short TAB of the measurements and the low permeabilities typical of claystones. It is possible that the shift is caused by drilling-induced fracture permeability in the vicinity of the borehole, which is seen at the shallow, rather than the deep, depth of investigation. The steplike increase in the resistivity log is not reflected in the other logs, but it does correlate with a smectite-rich zone (up to 90% smectite) that overlies the structurally defined prodecollement zone at Site 672.

Log Unit 2 is characterized by a well-defined low in the photoelectric effect, resistivity, total gamma-ray, and density logs, and by a slight increase in the neutron porosity log. This unit correlates with the upper part of lithologic Subunit IIB, which is a radiolarian-bearing siliceous claystone. The low photoelectric effect and density could be related to a higher concentration of opaline silica; however, the high neutron porosity and low resistivity in this unit suggest that the logs are influenced mainly by increased pore space. Relatively

high plagioclase within this unit reflects the presence of ash, which also contributes to the low photoelectric effect values.

Log Unit 3 correlates with the interval from the lower part of lithologic Subunit IIB to the base of Unit III. The high-resistivity interval at the top of log Unit 3 correlates with an increase in total clay, especially smectite. Starting at 210 mbsf are strong alternations in gamma ray and photoelectric effect. This depth corresponds to the top of lithologic Subunit IIC, comprising interbedded quartz-rich intervals and claystones. This oscillating behavior continues through lithologic Unit III, where there are interbedded marlstones and claystones, as reflected in the logs by an anticorrelation between the gamma-ray and photoelectric effect logs. From 310 to 335 mbsf there are decreasing trends in density and total gamma-ray values and low photoelectric effect values relative to the upper part of the section; however, there is no obvious lithologic signature that corresponds to the change in log character.

Log Subunits 4a and 4b correlate with lithologic Unit IV and are generally characterized by cyclically bedded sediments and higher concentrations of sand and carbonate than in Unit III. The spiky variability in the density and photoelectric effect logs is attributed at least in part to borehole washouts. Sands become an important sediment component at ~350 mbsf in Hole 672A, which is ~15 m below the first appearance of significant borehole enlargement in Hole 1044A. Given the presence of less cohesive lithologies in the vicinity of the washouts and the absence of change in drilling parameters, it seems likely that the enlargement is lithologically controlled. Log Subunit 4b is characterized by broad variations in photoelectric effect, resistivity, neutron porosity, and gamma-ray logs, that correlate well with the presence of turbidites and thick sand beds. The overall decrease in total gamma ray through log Unit 4 seems to correlate with the increase in the percentage of carbonate. Log Subunit 4c correlates in depth with the top of lithologic Unit V and is characterized by smaller amplitude variation in all the logs.

Log Unit 5 is the deepest interval that can be correlated with the Site 672 core data. The low photoelectric effect in log Subunit 5a correlates with low carbonate content and a high percentage of biogenic silica, which also are reflected in the lower density log values. Total clay content is quite high, according to the XRD data. The lower subunits of log Unit 5 can be compared only with Site 543, which is condensed relative to Site 672 because of a lower terrigenous component. The increase in total gamma ray in log Subunit 5b may be correlated with a zeolite-rich interval in the middle lower Eocene at Site 543, implying a similar sedimentation rate at Sites 543 and 1044 in the early Eocene.

Log Unit 6 is the lowermost unit at Site 1044 and is known to overlie Cretaceous basement. Lithologies of this age recovered at Site 543 are dolomitized calcareous ferruginous claystones. The high degree of variability in the logs—particularly the gamma ray, resistivity, and density—may be related to a high degree of hydrothermal alteration in sediments similar to those recovered at Site 543. The broad peak in the total gamma ray that defines log Subunit 6a is caused mainly by a large increase in thorium; however, there is no discernible correlation with lithologic features. The increase in density at 615 mbsf probably marks the top of the Cretaceous section and the presence of carbonates.

LOGS AND STRUCTURE

This section reviews core structural geology data presented in the “Site 672” chapter of the Leg 110 *Initial Reports* volume (Shipboard Scientific Party, 1988) and relates it to LWD log character.

Bedding is horizontal to gently dipping ($<20^\circ$) through most of Hole 672A, with the exception of two narrow intervals with dips up to 80° at 190 and 385 mbsf (Fig. 10). Fault density is relatively high at the upper interval, and bedding rotation is inferred to result from

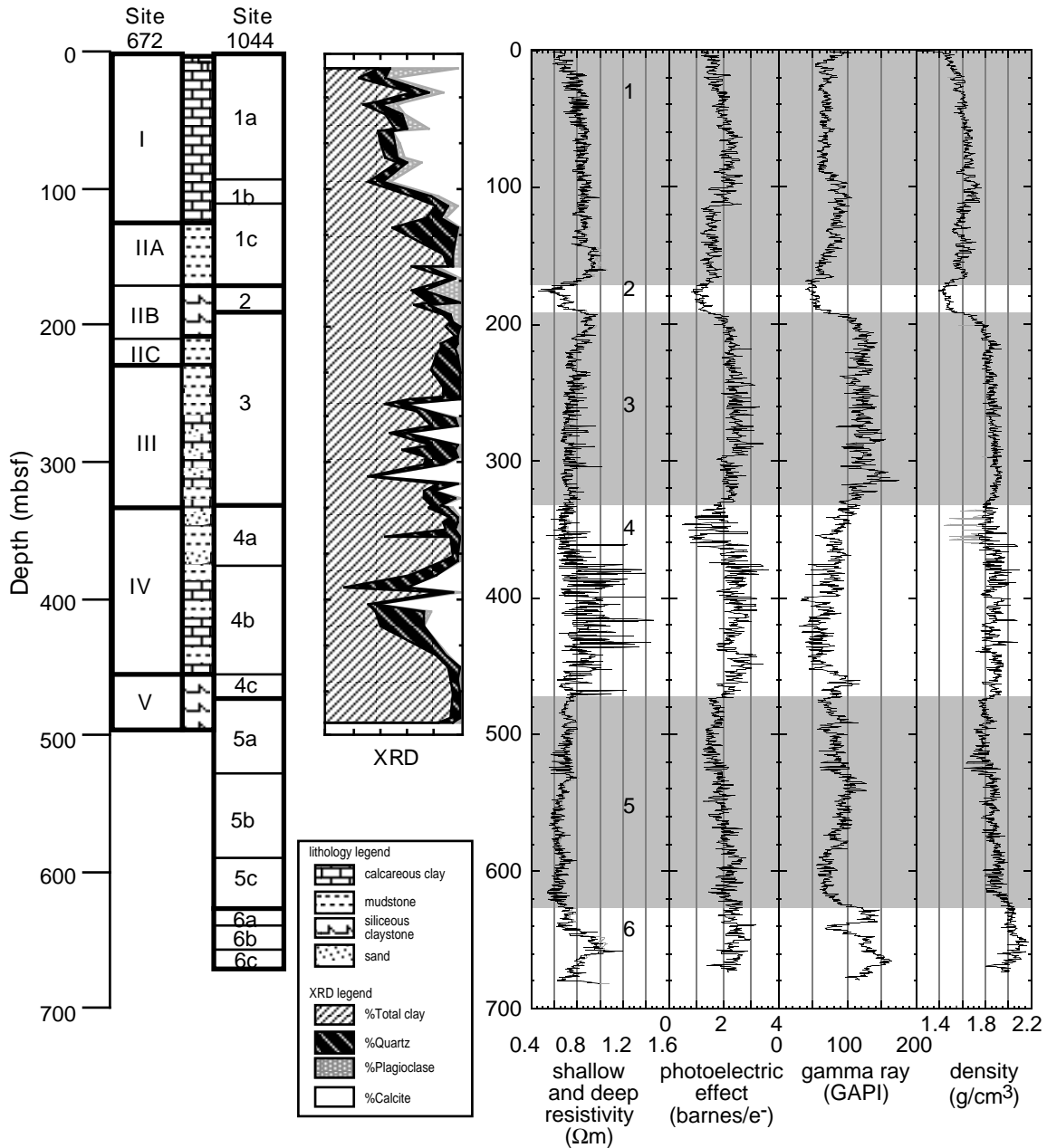


Figure 9. Summary of Site 1044 log units and Site 672 lithology data, including XRD mineralogy. The lithology column summarizes the major lithologic units described for Site 672 (Shipboard Scientific Party, 1988). Shaded areas in the log plot represent the boundaries of the major log units. The dark curve in the resistivity column = shallow resistivity; the light curve = deep resistivity. Both the edited and original versions of the density log are shown (see discussion of editing in the “Characterization of Logs” section, this chapter); the darker curve = the edited version.

tectonic activity. Several small normal faults in the lower interval may be responsible for the rotation of beds. Fault density is generally low through much of the hole, ranging from zero to one fault per 10 m of core. Two zones of relatively high fault density occur between 50 and 100 mbsf and between 175 and 200 mbsf. The upper zone consists of steeply dipping faults with predominately normal displacement. Subvertical dilation veins with clay-rich fill at the base of the zone of intense normal faulting are consistent with the stress geometry responsible for the faulting. The lower zone consists of moderately to gently dipping faults with reverse and normal displacement. The presence of one horizontal fault and two horizontal en echelon clay-filled vein arrays in this interval indicates subhorizontal shear. Irregular clay-filled vein networks and subvertical clay-filled veins are

also present. This zone was previously interpreted to represent a proto-décollement zone propagating within the Miocene sedimentary section ahead of the megascopic deformation front (Shipboard Scientific Party, 1988). The relationship between the normal faults and low-angle reverse faults is unresolved in cores.

As Site 1044 is about 35 m from Site 672, the position of the high-angle normal faults, determined from the seismic reflection data, varies between the two holes. It is therefore not possible to relate features in the LWD data to the position of normal faults in Hole 672A. The zone of relatively intense deformation between 175 and 200 mbsf, however, can be correlated and is approximately within log Unit 2 (Fig. 10). Recovery is about 50% through this interval, with abundant clay-filled veins within the core. The horizontal fault and en

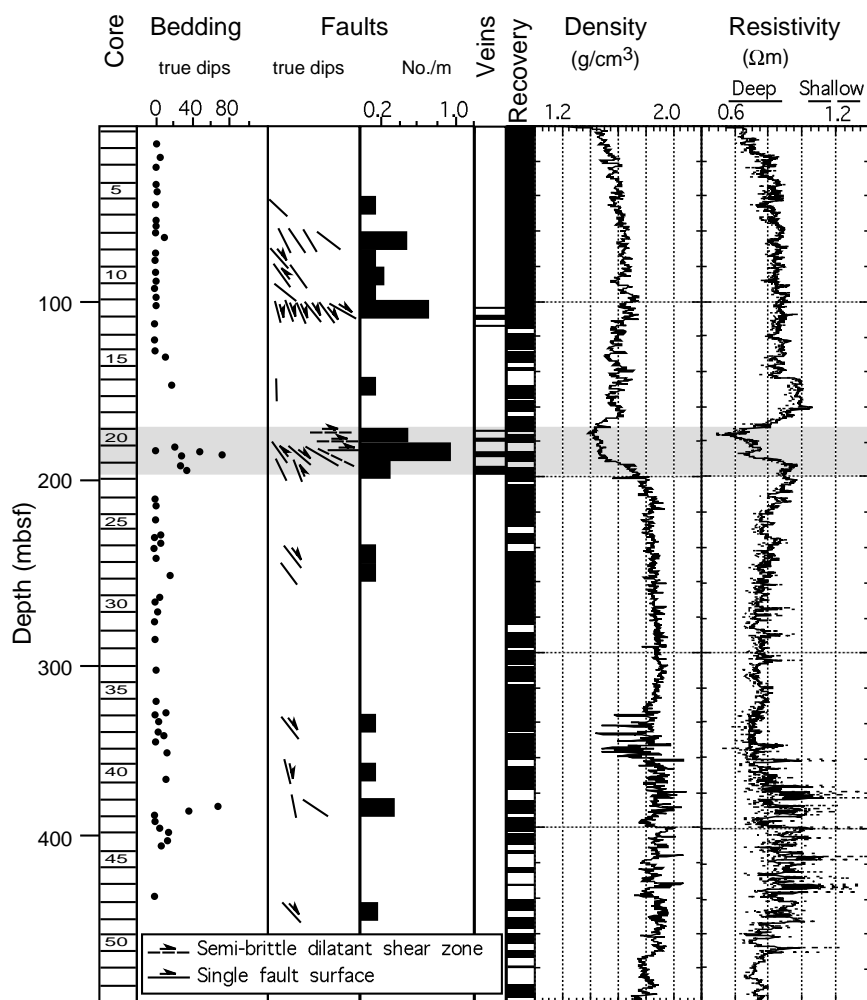


Figure 10. Structural synthesis of Hole 672A and correlation with Hole 1044A LWD logs. The position of the proto-décollement zone, defined by high density of small-scale faulting, is shown by shading.

echelon vein arrays occur in the upper section of lowest density and resistivity. The higher angle reverse and normal faults occur in the lower part of log Unit 2, which has relatively higher resistivity.

In summary, the incoming sediments are overprinted by two types of structures: high-angle normal faults throughout the section and a narrow interval of subhorizontal faults at the same stratigraphic level as the décollement zone within the prism. The normal faults are visible on seismic reflection lines and are correlated to variations in sea-floor morphology, suggesting active faulting. The subhorizontal shear zone correlates with a low in density and resistivity on the LWD logs. It is unclear whether the LWD signature is caused by structural features that are present or whether the deformation is localized in this zone because of the decreased strength of an undercompacted lithology that causes the LWD signature.

LOGS AND PHYSICAL PROPERTIES

Discussed within this section are the results of LWD relevant to the physical properties of the drilled section, particularly the downhole variability of the density and photoelectric effect logs. These logs are compared to index physical properties measurements derived from core from Site 672, where drilling penetrated the same sequence of sediments, and from Site 543, located 3.5 km seaward of the frontal thrust, but 18 km to the north. An additional objective for this site was to provide other shipboard investigations with a synthetic downhole porosity profile by integrating the density log at Site 1044 with grain density measurements from Sites 672 and 543.

Density

The downhole trend in bulk density between 0 and 110 mbsf (Table 2; Fig. 11A) is consistent with a normal consolidation trend, as was observed at Site 672 (Shipboard Scientific Party, 1988). The densities range from 1.4 to 1.7 g/cm³, with an average value of 1.60 g/cm³. From an apparent break at 110 mbsf in the downhole profile to 165 mbsf, the density varies between 1.65 and 1.50 g/cm³, with an average value of 1.58 g/cm³. Over the depth interval of 165 to 190 mbsf, bulk density drops sharply from 1.55 to 1.35 g/cm³ and then rises to 1.56 g/cm³, with an average value of 1.47 g/cm³. This anomalous interval of low bulk density coincides with the position of the structurally defined proto-décollement zone at Site 672. The density log across this zone is in excellent agreement with core bulk densities from Site 672 (Fig. 12). It is also consistent with other core physical properties and mineralogical studies, which have indicated lower smectite and higher quartz content and radiolarian tests in this interval (Shipboard Scientific Party, 1988; Tribble, 1990).

Below the proto-décollement zone down to 320 mbsf, bulk density values rise from average values of 1.65 g/cm³ to an overall average of 1.84 g/cm³. The observed downhole trend in density in this interval is consistent with the assumption of a normally consolidated sequence of calcareous claystone, as occurs at this depth at Site 672.

The density profile between 320 and 470 mbsf is strongly influenced by lithologic variation; namely, the occurrence of turbiditic sequences. The original (unedited) density data show a multitude of spikes as low as 1.45 g/cm³, which are considered artifacts because they correlate with zones of high differential caliper readings that

Table 2. Bulk density profile division with mean values and standard deviations.

Depth (mbsf)	Mean density (g/cm ³)	Standard deviation (g/cm ³)	Characteristics	Comments
0-110	1.60	0.07	Gradual rise	Normally compacted, homogeneous
110-165	1.58	0.04	Low constant value	Underconsolidated
165-190	1.47	0.04	Very low value	Proto-décollement horizon
190-320	1.84	0.05	Gradual rise	Normally consolidated homogeneous
320-470	1.85	0.07	Rapid large variations	Contrasting thin layers: turbidite beds
470-620	1.84	0.03	Gradual rise	Normally compacted
620-TD	2.03	0.04	Sharp rise/fall	Carbonate layers as in Site 543?

Note: TD = total depth.

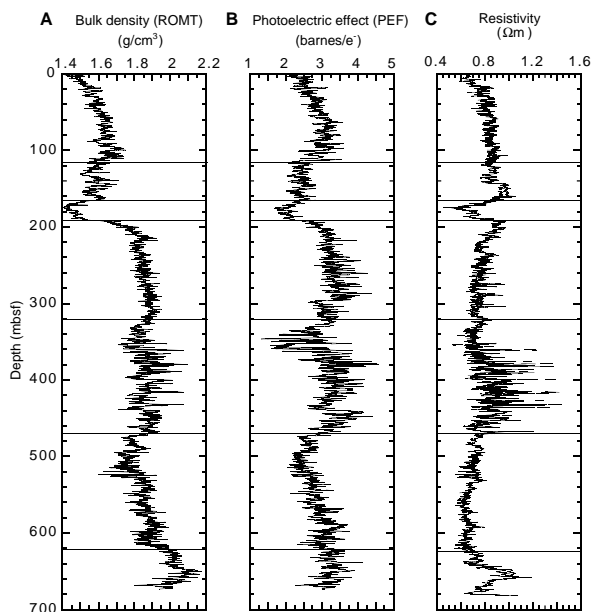


Figure 11. (A) Bulk density, (B) photoelectric effect, and (C) resistivity vs. depth in Hole 1044A. Lines separate intervals discussed in the text.

commonly exceed a threshold of 0.5 in (Fig. 13). In several instances, a specific low-density spike can be correlated with a silty or sandy layer recovered at Site 672 (Shipboard Scientific Party, 1988).

The interval from 470 to 620 mbsf shows a steady increase of bulk density with depth that appears to be modulated by lithologic variation; the overall average density is 1.84 g/cm³. The lowermost part of the density profile, from 620 mbsf to total depth, increases to a peak value of 2.15 g/cm³ and then decreases to an average density of about 1.95 g/cm³. The high densities are possibly caused by a sequence of hydrothermally altered carbonate-rich claystone similar to that recovered just above basement at Site 543.

Photoelectric Effect

As expected, the characteristics of the photoelectric effect down-hole profile closely match the trends observed in the density log (Fig. 11B). The photoelectric effect depends on the electron density, which correlates with the overall bulk density. Therefore, the divisions defined for the density log also apply to the photoelectric effect log.

Resistivity Log and Resistivity Porosity

A resistivity log can be an excellent porosity indicator. At Site 1044, the resistivity log curves (Fig. 11) increase significantly with depth in the upper 20 m of weakly consolidated sediments. Resistivity remains fairly constant at about 0.85 Ωm until about 142 mbsf, where the values increase and the deep (attenuation) resistivity is

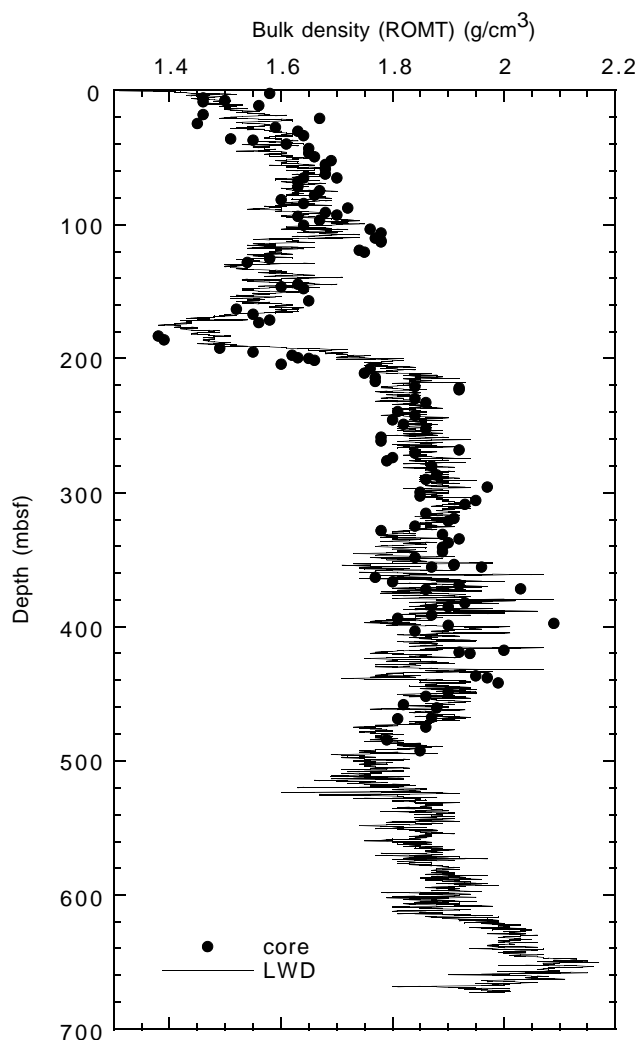


Figure 12. Bulk density vs. depth in Hole 1044A (solid line) superimposed on Site 672 wet bulk density from laboratory measurements on core (solid circles).

greater than the shallow resistivity. In the proto-décollement zone (log Unit 2), resistivity decreases by about 0.3 Ωm from Unit 1 and then increases beneath this zone. The resistivity values remain fairly constant at about 0.75 Ωm throughout log Unit 3 and Subunit 4a to 376.6 mbsf (top of log Subunit 4b), where high-resistivity spikes from turbidite units dominate. The resistivity log is less variable beneath the log Unit 4/5 boundary at 470.5 mbsf.

The resistivity porosity log is similar to the resistivity log. It is calculated using Archie's law, which relates the resistivity of the formation water, resistivity of the formation, and porosity (for details, see

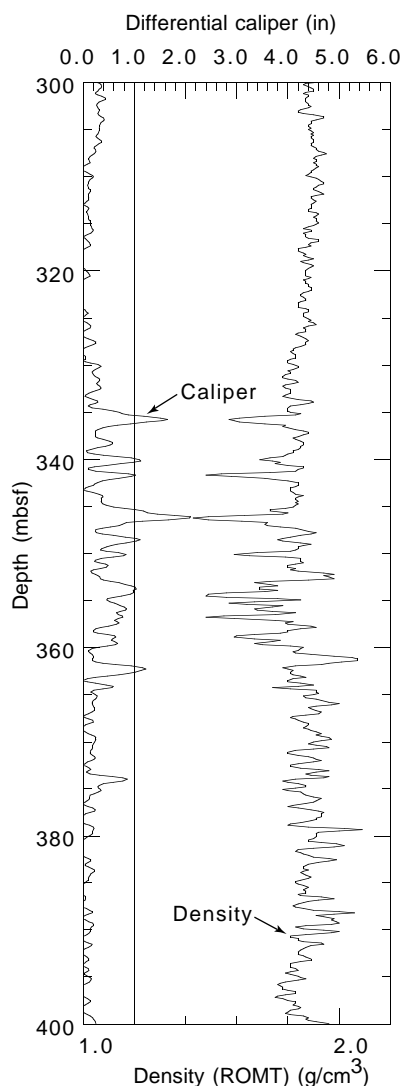


Figure 13. Comparison of the density and differential caliper logs between 300 and 400 mbsf shows a high degree of correlation between low-density spikes and differential caliper readings exceeding 0.5 in.

“Explanatory Notes” chapter, this volume). However, the resistivity porosity log is unlikely to be an accurate porosity log for this site. Site 1044 is clay rich, and conductive clay can cause resistivity to misrepresent porosity. The resistivity porosity log does not resemble the porosity log created from the bulk density log, which we believe is of excellent quality at this site.

Porosity Calculation From LWD Density Log

The density data obtained from LWD closely resemble the individual core wet bulk density measurements from Site 672, although at a much higher resolution (Fig. 12). To correct for the effects of borehole washouts between 330 and 370 mbsf (see “Characterization of Logs” section, this chapter), low-density spikes were removed before the porosity calculation. The calculated porosities are sensitive to the grain density used in the calculation. To check the effect of the variation of grain density on the calculated porosity profiles, two profiles were constructed and compared with the calculated porosity data from cores at Site 672 (Shipboard Scientific Party, 1988).

As a first approach, the grain density was assumed to be 2.75 g/cm³ throughout the profile, an assumption used during Leg 110

(Shipboard Scientific Party, 1988). A comparison of the porosity profile, calculated from LWD data, with the porosities from the Site 672 core shows a good match (Fig. 14), especially in the upper 200 m of the section. However, a grain density of 2.75 g/cm³ seems too high when compared with the measured grain densities at Site 672 (Shipboard Scientific Party, 1988). Also, it seems unlikely that the grain density would be constant over the entire depth of the hole, which penetrates a variety of lithologies. Therefore, a smoothed grain density profile was constructed by averaging measured grain densities from Site 672 to 618 mbsf for four depth intervals, separated by major offsets in the downhole grain density trends (Table 3; Fig. 15). The grain density for the lowermost part of Hole 1044A (618 mbsf to total depth) was estimated from the wet bulk density and porosity of Site 543 lithologic Unit VI (upper Maastrichtian to lower Campanian bioturbated, calcareous ferruginous claystone; Shipboard Scientific Party, 1984).

As the estimated grain densities used are lower than the average density of 2.75 g/cm³, the second calculated porosity profile (Fig. 16) is shifted to lower porosities, especially between 200 and 280 mbsf. The maximum and mean differences between these two profiles presented are ~9% and ~4%, respectively. Although the second calculated porosity profile appears to be more reliable, it should be used only with great caution for further quantitative applications such as hydrologic models. The calculation incorporates grain density data that are not as high in quality as the density log. Moreover, as Brown and Ransom (1996) showed, the conventional porosity determinations conducted in the physical properties laboratory during ODP cruises tend to overestimate the porosity of sediments that contain abundant hydrous minerals such as smectite. As much as 25% of the mineral mass of smectite can be made up of H₂O, which resides in smectite interlayers. This water is easily removed through oven drying or exposure to low humidities, leading to erroneous calculations of porosity and water content. As some parts of the section are known to be extremely rich in smectite, this observation should be considered and appropriately factored into porosity calculations.

Summary

1. The density log agrees well with core bulk densities from Site 672.
2. The density log delineates a low-density interval correlating with the proto-décollement zone.
3. The resistivity log is not a useful tool for deriving a porosity profile at this site.
4. The porosity profiles, calculated from unreliable grain density data from previously drilled core, are of poor quality.

LOGS AND INDICATORS OF FLUID FLOW

Anomalous values in chemical and thermal data collected during Leg 110 were used to infer lateral fluid migration flow from beneath the accretionary complex to Site 672. Proposed fluid-flow paths consist of a proto-décollement zone located between 170 and 220 mbsf and multiple sand layers within a turbidite sequence at 332–455 mbsf. In this section, we discuss the LWD results from these proposed fluid-flow paths.

Site 1044 LWD data and Site 672 chemical data are presented in Figure 17. In addition, estimates of pore-pressure conditions at Site 672 are shown. The pore pressure is normalized according to the definition of λ^* given in the “Explanatory Notes” chapter (this volume). Pore pressures were inferred from the results of laboratory consolidation tests of core samples by Taylor and Leonard (1990). The preconsolidation stress was interpreted to be the maximum effective overburden load that the sediment had experienced. Excess pore pressures were calculated by subtracting the preconsolidation stress from the estimated lithostatic load (Taylor and Leonard, 1990). Lateral stress-

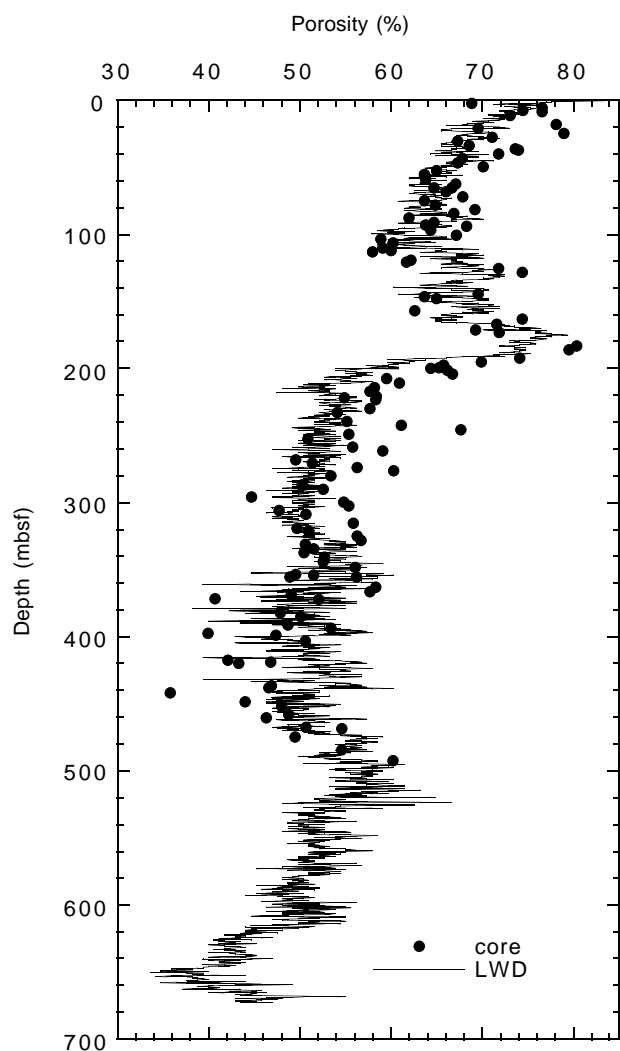


Figure 14. Porosity profile (solid line) calculated from the Hole 1044A bulk density profile and a constant grain density of 2.75 g/cm³, with porosity measurements from Site 672 core (solid circles).

Table 3. Grain densities used for the construction of a synthetic porosity profile.*

Depth (mbsf)	Estimated grain density (g/cm ³)	Reference (mbsf)
0-130	2.7	Site 672 (0-130)
130-265	2.56	Site 672 (130-265)
265-410	2.63	Site 672 (265-410)
410-618	2.53	Site 672 (410-492)
618-TD	2.76	Site 543 (380-410)

Notes: * = see text for discussion; TD = total depth.

es were not considered in this estimate, which may be a reasonable assumption at Site 672 because it is seaward of the frontal thrust. The calculated λ^* values indicate that sediments are overconsolidated near the seafloor and become underconsolidated from 55 to 200 mbsf (Taylor and Leonard, 1990).

Proto-Décollement Zone (Log Unit 2)

At Site 672, the proto-décollement zone was identified based on an increase in porosity and on observations of veins and subhorizon-

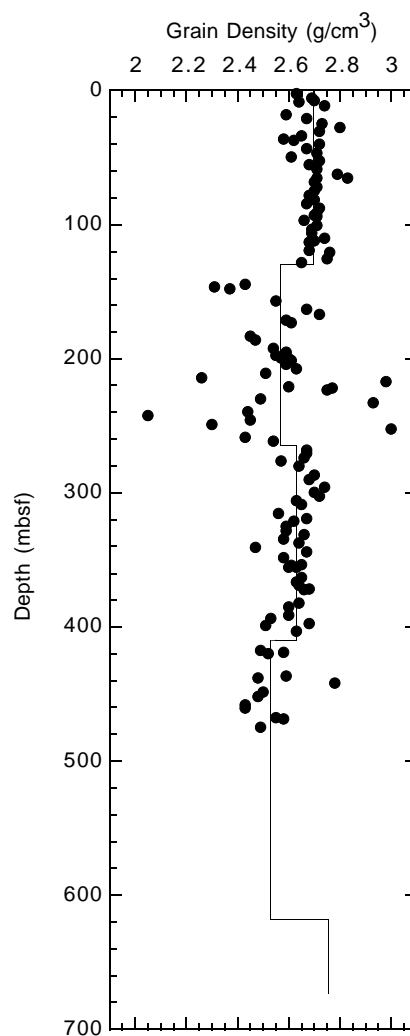


Figure 15. Grain densities from Sites 672 and 543 (solid circles) averaged over five depth intervals (vertical lines).

tal shear fabrics over the interval 170–200 mbsf (Shipboard Scientific Party, 1988). Lithologic characterization of this zone suggests reduced total clay content, low smectite (Tribble, 1990), and greater amounts of radiolarians compared with the sediments immediately above and below. The structurally defined proto-décollement zone correlates with log Unit 2 at Site 1044, which has low bulk density and resistivity (Fig. 17).

Hydrogeologically, because of its higher porosity (lower bulk density) and lower clay content, Unit 2 could reasonably be inferred to have higher permeability than the surrounding units. However, several lines of evidence suggest that this unit might not carry a significant volume of flow from beneath the accretionary complex. First, this zone is not associated with a clear chemical anomaly. The chloride concentration of a sample collected from the center of this zone (185 mbsf) is slightly greater than that of seawater. There is an extensive geochemical discussion in the Leg 110 *Initial Reports* volume (Shipboard Scientific Party, 1988) regarding the validity of the chloride concentration measured in the proto-décollement zone. Based on the concentration of its other major constituents, the sample did not appear to be contaminated, and the value appears to be valid. The closest observed values of low chloride and high methane are located 26 m below the base of this zone. In the context of the intermittent spacing of core samples from Site 672, it was inferred that the pore-water anomalies at 216 mbsf are related to the structural features observed in the interval from 170 to 190 mbsf. However, the log data

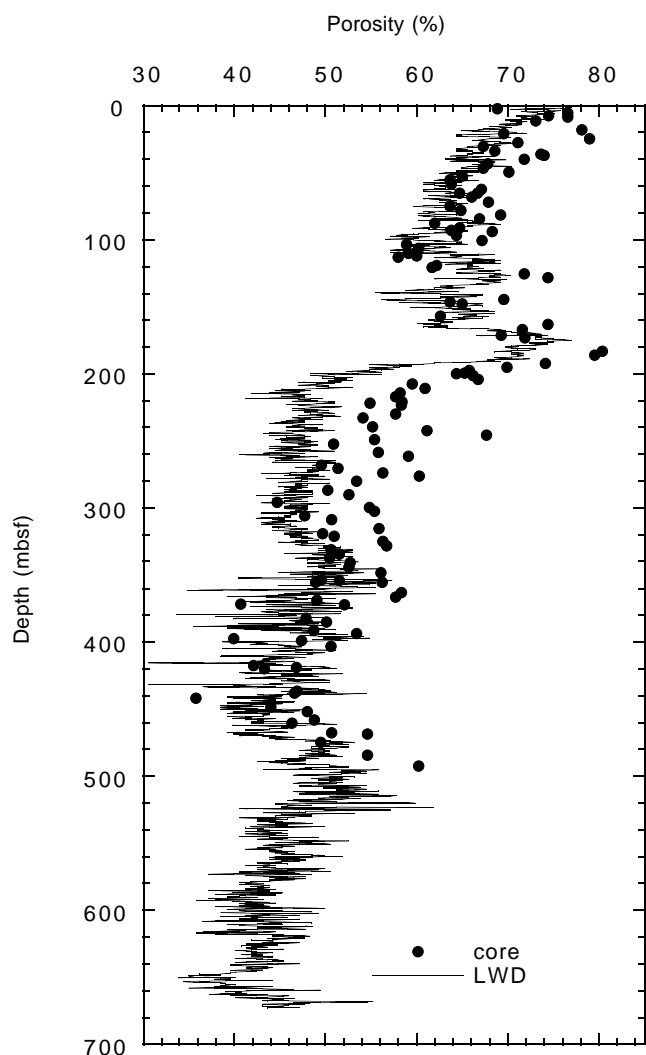


Figure 16. Porosity profile calculated from the Hole 1044A bulk density profile (solid line) and average grain densities from Sites 672 and 543 (Table 3; Fig. 15; see text for discussion), with porosity measurements from Site 672 core (solid circles).

provide a continuous picture of the sediment properties in which the relationship between Unit 2 and the geochemical anomalies measured 26 m below its base is less clear.

A second problem with the case for significant flow in the proto-décollement zone is that the high porosities over this interval can be attributed to causes other than the presence of pressured fluid from the accretionary complex. Unit 2 is overlain and underlain by smectite-rich layers (log Subunit 1c and Unit 3, respectively). Low permeability within these layers may have limited the consolidation rate of Unit 2, thereby creating overpressures. Excess pore pressures estimated from samples suggest overpressuring directly above Unit 2 (Taylor and Leonard, 1990). Alternatively, Wilkens et al. (1990) suggested that the observed high porosities may not be caused by overpressuring, but may be indicative of different lithologies. Radiolarian tests may hold open the sediment framework, allowing higher porosities than expected for clays at this depth.

A third line of evidence suggesting that the proto-décollement zone may not be a major fluid conduit is provided by the comparison of temperature measurements from Site 672 (Shipboard Scientific Party, 1988) and Site 543 (Shipboard Scientific Party, 1984), located

18 km to the north. Temperature measurements from Site 672 indicate a thermal gradient of 79°C/km. The deepest temperature determination was at 133.8 mbsf. These temperatures correspond to an estimated heat flow of 92 mW/m², 80% higher than expected for 90-Ma oceanic crust (Fisher and Hounslow, 1990). Based on the high thermal gradient at Site 672, Fisher and Hounslow (1990) suggested several possible locations for conduits for the migration of warm fluids: (1) the proto-décollement zone at ~190 mbsf, (2) a sand layer at 370 mbsf, or (3) a sand layer at 450 mbsf.

In contrast, a thermal gradient of about 30°C/km was estimated at Site 543 (Davis and Hussong, 1984). This low heat flow suggests that, unlike at Site 672, migration of warm fluids has not occurred recently at Site 543. If the proto-décollement zone were the major fluid conduit at Site 672, elevated heat flow should also be expected at Site 543, where the higher porosity, radiolarian-rich zone was also observed. Coarse-grained turbidite deposits are absent at Site 543, possibly because the Tiburon Rise acted as a barrier to northward turbidite transport (Dolan et al., 1990). Therefore, the sand layers at Site 672 are more likely to provide the fluid migration pathways.

Turbidite Deposits (Log Unit 4)

A sequence of alternating high and low densities and resistivities was imaged in log Unit 4. In general, chloride concentrations are low and methane is elevated within this unit, which corresponds to a series of turbidites. In particular, chloride concentrations as low as 10% fresher than seawater were observed at ~320 and 450 mbsf; an increase in methane concentration to 200 mM was observed at ~420 mbsf, and values of $\delta^{18}\text{O}$ that are 2‰–3‰ above the depth trend were observed at ~320 and 450 mbsf (Fig. 17). Flow is most likely to occur within sand-rich layers of the turbidite sequence that are laterally connected. The chemical and thermal profiles are consistent with advective flow along several thick, high-permeability layers and with diffusive transport within the intervening low-permeability layers.

Summary

1. Although the LWD logs indicate that the proto-décollement zone has low bulk density and resistivity, the location of previously established geochemical anomalies does not correlate with this zone.
2. Strong oscillations in density and resistivity in log Unit 4 clearly image a series of turbidite sequences. Geochemical and thermal data suggest that sand layers within these turbidites transmit significant flow from beneath the accretionary complex.

LOGS AND SEISMIC DATA

Synthetic Seismogram

The synthetic seismogram (Fig. 18) was constructed using an assumed velocity profile as described in the “Explanatory Notes” chapter (this volume). At Site 1044 the velocity profile consists of a linear gradient from 1.5 km/s at the seafloor to 2.0 km at the top of the oceanic crust.

The four main seismic units on Line 751, identified by Moore et al. (1995) are reasonably well correlated with the synthetic seismogram (Fig. 18). These units consist of an interval of moderate to strong reflections from the seafloor to 5190 mbsl (230 mbsf), a very low reflectivity interval from 5190 to 5360 mbsl (230–400 mbsf), a series of moderate reflections between 5360 and 5480 mbsl (400–520 mbsf), and a nonreflective interval from 5480 mbsl (520 mbsf) to the bottom of the hole at 5633 mbsl (673 mbsf) (Fig. 4). A series of reflections produced from the low-density proto-décollement interval are particularly noteworthy in comparison with the synthetic trace. The waveforms of the synthetic and data traces appear to match rea-

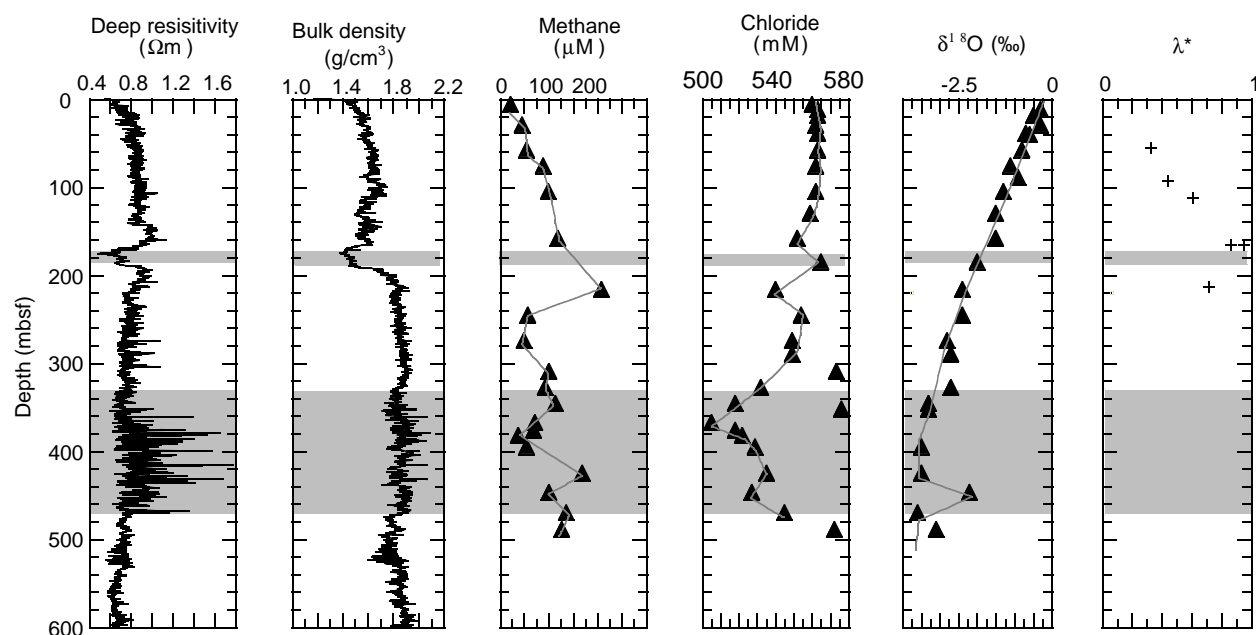


Figure 17. Comparison of LWD data from Hole 1044A with geochemical and pore-pressure results from Site 672. The upper shaded area indicates log Unit 2, which correlates with the proto-décollement zone. The lower shaded area indicates log Unit 4, which correlates with the series of turbidites. Curves drawn for the methane and chloride concentration-depth profiles are based on the interpretation of Gieskes et al. (1990). The curve for the $\delta^{18}\text{O}$ profile is based on the interpretation of Vrolijk et al. (1990).

sonably well in amplitude and character from about 5100 to 5180 mbsl, indicating that several low-density intervals between 100 and 200 mbsf in the LWD logs are the cause of this series of reflections. The lateral continuity of this reflection in the undeformed sediment sequence seaward of the deformation front indicates that the low-density interval is regionally significant. By comparison to seismic models of the décollement zone (Bangs et al., 1996), the proto-décollement and décollement reflections are caused by similar low-impedance intervals. However, the top and bottom interfaces of the proto-décollement low-impedance layer are probably more diffuse than along the décollement zone, resulting in a weaker proto-décollement reflection. The lateral variability of the proto-décollement reflection suggests greater lateral variations in thickness and sharpness of the proto-décollement layer interfaces than that observed along the décollement zone.

REFERENCES

- Bangs, N.L.B., Shipley, T.H., and Moore, G.F., 1996. Elevated fluid pressures and fault zone dilation inferred from seismic models of the northern Barbados Ridge décollement. *J. Geophys. Res.*, 101:627–642.
- Biju-Duval, B., Moore, J.C., et al., 1984. *Init. Repts. DSDP, 78A*: Washington (U.S. Govt. Printing Office).
- Brown, K.M., and Ransom, B., 1996. Porosity corrections for smectite-rich sediments: impact on studies of compaction, fluid generation, and tectonic history. *Geology*, 24:43–84.
- Davis, D.M., and Hussong, D.M., 1984. Geothermal observations during Deep Sea Drilling Project Leg 78A. In Biju-Duval, B., Moore, J.C., et al., *Init. Repts. DSDP, 78A*: Washington (U.S. Govt. Printing Office), 593–598.
- Dolan, J.F., Beck, C., Ogawa, Y., and Klaus, A., 1990. Eocene-Oligocene sedimentation in the Tiburon Rise/ODP Leg 110 area; an example of significant upslope flow of distal turbidity currents. In Moore, J.C., Mascle, A., et al., *Proc. ODP, Sci. Results*, 110: College Station, TX (Ocean Drilling Program), 47–83.
- Fisher, A.T., and Hounslow, M.W., 1990. Heat flow through the toe of the Barbados accretionary complex. In Moore, J.C., Mascle, A., et al., *Proc.*

- ODP, Sci. Results*, 110: College Station, TX (Ocean Drilling Program), 345–363.
- Gieskes, J.M., Vrolijk, P., and Blanc, G., 1990. Hydrogeochemistry, ODP Leg 110: an overview. In Moore, J.C., Mascle, A., et al., *Proc. ODP, Sci. Results*, 110: College Station, TX (Ocean Drilling Program), 395–408.
- Mascle, A., and Moore, J.C., 1990. ODP Leg 110: tectonic and hydrologic synthesis. In Moore, J.C., Mascle, A., et al., *Proc. ODP, Sci. Results*, 110: College Station, TX (Ocean Drilling Program), 409–422.
- Mascle, A., Moore, J.C., et al., 1988. *Proc. ODP, Init. Repts.*, 110: College Station, TX (Ocean Drilling Program).
- Moore, G.F., Zhao, Z., Shipley, T.H., Bangs, N., and Moore, J.C., 1995. Structural setting of the Leg 156 area, northern Barbados Ridge accretionary prism. In Shipley, T.H., Ogawa, Y., Blum, P., et al., *Proc. ODP, Init. Repts.*, 156: College Station, TX (Ocean Drilling Program), 13–27.
- Shipboard Scientific Party, 1988. Site 672. In Mascle, A., Moore, J.C., et al., *Proc. ODP, Init. Repts.*, 110: College Station, TX (Ocean Drilling Program), 205–310.
- , 1984. Site 543: Oceanic reference site east of the Barbados Ridge complex. In Biju-Duval, B., and Moore, J.C., et al., *Init. Repts. DSDP, 78A*: Washington (U.S. Govt. Printing Office), 227–298.
- Taylor, E., and Leonard, J., 1990. Sediment consolidation and permeability at the Barbados forearc. In Moore, J.C., Mascle, A., et al., *Proc. ODP, Sci. Results*, 110: College Station, TX (Ocean Drilling Program), 289–308.
- Tribble, J.S., 1990. Clay diagenesis in the Barbados accretionary complex: potential impact on hydrology and subduction dynamics. In Moore, J.C., Mascle, A., et al., *Proc. ODP, Sci. Results*, 110: College Station, TX (Ocean Drilling Program), 97–110.
- Vrolijk, P., Chambers, S.R., Gieskes, J.M., and O'Neil, J.R., 1990. Stable isotope ratios of interstitial fluids from the northern Barbados accretionary prism, ODP Leg 110. In Moore, J.C., Mascle, A., et al., *Proc. ODP, Sci. Results*, 110: College Station, TX (Ocean Drilling Program), 189–205.
- Wilkins, R., McLellan, P., Moran, K., Tribble, J.S., Taylor, E., and Verduzco, E., 1990. Diagenesis and dewatering of clay-rich sediments, Barbados accretionary prism. In Moore, J.C., Mascle, A., et al., *Proc. ODP, Sci. Results*, 110: College Station, TX (Ocean Drilling Program), 309–320.

Ms 171AIR-103

NOTE: For all sites drilled, shore-based log processing data are available on CD-ROM. See Table of Contents for material contained on CD-ROM.

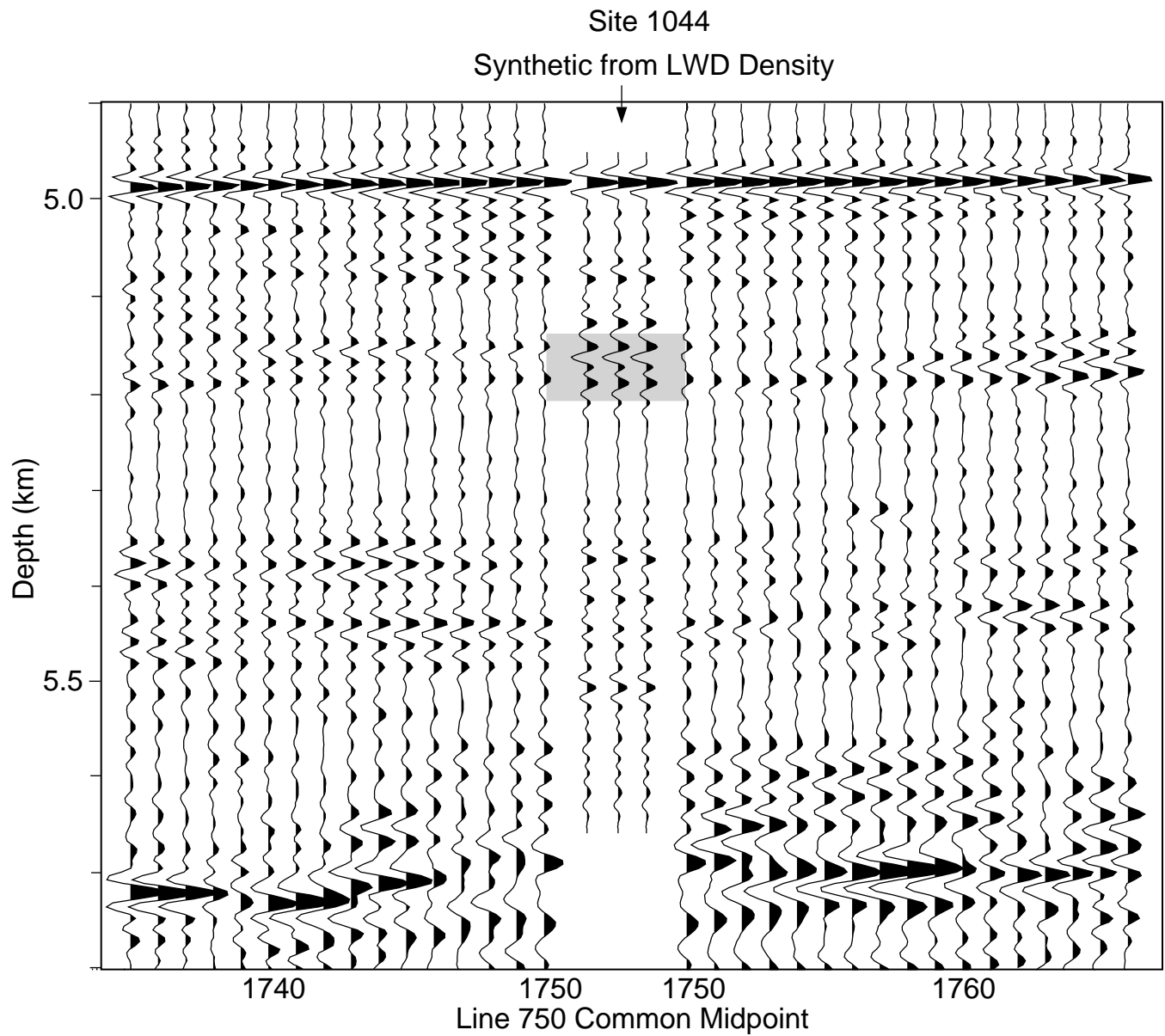


Figure 18. Three identical synthetic traces are shown at Site 1044 on Line 750. The shaded area shows the location of the proto-décollement zone, as indicated by the density log. See the “Explanatory Notes” chapter (this volume) for a description of the synthetic seismogram construction.